ESTIMATION OF PROTECTION FACTORS FOR THE TRANSPORT OF RADIOACTIVE MATERIAL

A Thesis

by

SENA DALAK

Submitted to the Office of Graduate and Professional Studies of
Texas A&M University
in partial fulfillment of the requirements for the degree of

MASTER OF SCIENCE

Chair of Committee,	Shaheen Azim Dewji
Committee Members,	John Ford
	Xiaofeng Nie
Head of Department,	Michael Nastasi

August 2021

Major Subject: Nuclear Engineering

ABSTRACT

In the event of exposures from contamination events resulting from transportation of radioactive materials, the radiation protection factor (RPF) value of a vehicle informs emergency responders and the general public about protection level of a vehicle. Prior studies evaluating RPFs demonstrate a lack of realistic vehicle configurations and the results cannot be extended directly to scenarios when a vehicle is surrounded by a contaminated environmental field or internally contaminated with a field in-cabin. Consequently, there is further need to determine the exposure risk to first responders, the workforce crew, and civilians for early-phase protection actions or controlling the contaminated transportation routes, as the presence of radiation will not be known until trained personnel with specialized equipment are on the scene. Transportation risk analysis code, RADTRAN, simplifies incident-free population dose from external radiation emitted by radioactive material packages using simplified mathematical models. In terms of simplified mathematical models, as the code over-estimates the dose from experimental calculations, there is a need for updating the previous validations to point out better the differences between the models for different scenarios. An analysis of the simplified mathematical models used in transportation risk code for incident-free transportation and the RPF values for vehicles under hypothetical accident/incident condition of transport will help to increase the reliability of the RADTRAN transport code and utility of RPF values for vehicle, respectively, which will result in improved radiation protection protocol in handling and consequence management scenarios.

ACKNOWLEDGEMENTS

I would like to thank to my committee chair, Dr. Dewji, and my committee members, Dr. Ford, and Dr. Nie, for their guidance and support throughout the course of this research. I would also like to thank Dr. Wesley Bolch and Dr. Nina Petoussi-Henss for providing supplemental information regarding ICRP environmental exposure data.

Thanks also go to my friends and colleagues and the department faculty and staff for making my time at Texas A&M University a great experience.

Finally, thanks to my mother, father, and brother for their encouragement and to my boyfriend for his support and love.

Graduate study was supported by the Republic of Turkey Ministry of National Education.

CONTRIBUTORS AND FUNDING SOURCES

Contributors

All other work conducted for the thesis was completed by the student with the support and advising of her Chair and Committee.

Funding Sources

No external funding was received for the research and completion of this thesis.

TABLE OF CONTENTS

Page

ABSTRACT ii

ACKNOWLEDGEMENTS iii

CONTRIBUTORS AND FUNDING SOURCES iv

TABLE OF CONTENTS v

LIST OF FIGURES vii

LIST OF TABLES ix

1. INTRODUCTION 1

2. BACKGROUND 5

2.1. Dose Calculations 5
2.2. Computational Phantoms 7
2.3. Transportation Dose Limit and Transport Index 9
2.4. RADTRAN Transport Risk Analysis Code 10
2.5. Radiation Protection Factor for Vehicle 15
2.6. Environmental Contamination 19

3. OBJECTIVE 21

4. METHODOLOGY 23

4.1. Incident-free Condition of Transport 23
4.1.1. Type A Package 24
4.1.2. RADTRAN Analysis 25
4.2. Hypothetical Incident Condition of Transport 26
4.2.1. Vehicle Models 28
4.2.2. Contaminated Scenario Calculations 29
4.2.2.1. Soil Contamination 30
4.2.2.1.1. Geometry Overview 30
4.2.2.1.2. Soil Composition and Ground Characteristics 33
4.2.2.1.3. Photons and Dose Calculations 34
4.2.2.2. Air Contamination 35

4.2.2.2.1. Geometry Overview 35
4.2.2.2.2. Air Composition 37
4.2.2.2.3. Photons and Dose Calculations 37
4.2.2.3. Trailer Contamination 38
4.2.3. Unshielded Dose Calculations 40
4.2.4. Variance Reduction 40
4.2.5. RPF Calculations 41

5. RESULTS 43

5.1. Incident-free Condition of Transport 43
5.2. Hypothetical Incident Condition of Transport 46
5.2.1. Benchmarking 46
5.3. Shielded and Unshielded Effective Dose Rates 47
5.3.1. Radiation Protection Factors 49
5.3.1.1. Radionuclide-specific Protection Factors 53

6. DISCUSSIONS 55

6.1. RADTRAN Analysis 55
6.2. RPF 56

7. CONCLUSION 61

REFERENCES 63

APPENDIX A – SIMULATION PARAMETERS 66

LIST OF FIGURES

Page

Figure 1. A radioactive material package label. 10

Figure 2. Critical dimension of the transportation package used in RADTRAN. 12

Figure 3. Modeled package and a phantom used in incident-free simulations. 24

Figure 4. Cylinder used in SSW step representing the coupling surface for soil contamination. 32

Figure 5. The vehicle model with phantom inside of the coupling surface used in SSR step. 32

Figure 6. Cylinder and air cube used in SSW step for air contamination. 36

Figure 7. Truck-trailer used in SSW step for trailer contamination. 39

Figure 8. Dose rate as a function of source-to-receptor distance resulted from RADTRAN, effective dose rate resulted from modeled Type A package with phantom, and simplified point and line source models. 44

Figure 9. Dose rate as a function of source-to-receptor distance resulted from RADTRAN, effective dose rate resulted from modeled Type A package with phantom, and simplified line source model. 45

Figure 10. Dose rate as a function of source-to-receptor distance resulted from RADTRAN, effective dose rate resulted from modeled Type A package with phantom, and simplified point source model. 45

Figure 11. Sex-averaged effective dose rate coefficients for soil contamination. Also shown are the results of FGR 15 and ICRP 144. 46

Figure 12. Sex-averaged effective dose rate coefficients for air contamination. Also shown are the results of FGR 15 and ICRP 144. 47

Figure 13. Sex-averaged effective dose rate coefficients for soil contamination for unshielded and shielded phantom. Shielded phantom results are shown for 1-cm-thick box, 1-in-thick box, and more realistic vehicle model. 48

Figure 14. Sex-averaged effective dose rate coefficients for air contamination for unshielded and shielded phantom. Shielded phantom results are shown for 1-cm-thick box, 1-in-thick box, and more realistic vehicle model. 48

Figure 15. Sex-averaged effective dose rate coefficients for truck-trailer contamination for unshielded and shielded phantom. Shielded phantom results are shown for 1-cm-thick box, 1-in-thick box, and more realistic vehicle model. 49

Figure 16. Calculated radiation protection factors for soil contamination for 1-cm-thick box, 1-in-thick box, and more realistic vehicle model. 50

Figure 17. Calculated radiation protection factors for air contamination for 1-cm-thick box, 1-in-thick box, and more realistic vehicle model. 50

Figure 18. Calculated radiation protection factors for truck-trailer contamination for 1-cm-thick box, 1-in-thick box, and more realistic vehicle model. 51

Figure A-1. PIMAL mathematical phantom model used as a representative driver…… 66

Figure A-2. 1-cm-thick and 1-in-thick box model…… 68

Figure A-3. More realistic vehicle model…… 69

Figure A-4. Truck-trailer model……..... 69

LIST OF TABLES

Page

Table 1. Radiation weighting factor values for different radiation types. 6

Table 2. Tissue weighting factors for organ and tissues. 7

Table 3. Dose reduction factors of vehicle converted into RPF for cloudshine for various photon energies. 18

Table 4. Dose reduction factors of vehicle converted into RPF for groundshine for various relaxation mass depths considering only the contribution of ^{137}Cs. 18

Table 5. Modeled Type A package parameters. 25

Table 6. Details of method used for contaminated environment simulations. 30

Table 7. Soil composition. 33

Table 8. Air composition. 37

Table 9. Generated radionuclides for RPF values. 42

Table 10. Energy values where the protection factor is equal to about 2. 51

Table 11. Percentage of unprotected dose rate received from 2 MeV photons 52

Table 12. Calculated stay time to reach NCRP dose limits in a vehicle, 1-cm-box, and 1-in-box from Fukushima contamination scenario for the reference maximum deposition density. 52

Table 13. Radionuclide-specific RPFs. 53

Table A-1. Fiberglass composition used in vehicle window 67

Table A-2. Steel composition used for Type A package 67

Table A-3. Carbon Steel composition used for vehicles 68

Table A-4. Photon energy and intensity data for generated radionuclides 70

1. INTRODUCTION

With the use of radioactive material (RAM) in numerous fields outside of nuclear energy fuel cycle activities, such as nuclear medicine, defense, decommissioning, and academic research, transportation of these materials is becoming increasingly prevalent. Transportation of RAM for these various industries are primarily conducted by highway travel, although there are several options including rail. As a result, the transportation of radioactive material continues to remain a safety priority given potential hazards involved in transferring the package from one location to another. One approach to address these concerns is by using environmental impact and risk assessment codes for analyzing and improving the transportation of radioactive and other hazardous materials. In the past few decades, environmental impact and risk assessment codes that assess RAM transportation, such as RADTRAN [1] and RISKIND [2], have been an area of focus for greater development. Dating back to the 1970s, development of such capabilities at facilities such as Sandia National Laboratories (SNL) have made improvements by adopting new simplified mathematical models to estimate radiation dose to workers and members of the public. SNL initially released a simplified mathematical model in 1977 termed the RADionuclide Transport, Removal, And Dose (RADTRAD) estimation code [3], which was the first iteration of RADTRAN in conjunction with NUREG-0170 [4].

In the event of radiological incident involving the release of RAM - whether accidental or from a malicious event - it may be crucial to estimate doses to individuals who are transported through contaminated areas by vehicles and the dose to operators of

the transportation vehicles. To this extent, the radiation protection factor (RPF) can be obtained for different types of vehicles, which indicates the protection level of the vehicle from external radiation sources. Each measurement is dependent on thickness and composition of the shielding and the source contaminant radiation type and energy. Applicable to both military and civilian vehicles, specific RPF is determined from the ratio of unshielded radiation dose outside in comparison with the shielded dose present within the vehicle, as shown in Equation 1:

$$RPF = \frac{Unshielded\ Dose\ (neutron + gamma)}{Shielded\ Dose\ (neutron\ +\ gamma)} \qquad Eq.1$$

As the value of RPF increases, the greater the dose reduction due to shielding is provided by the vehicle. The RPF value is above 1 means that person inside of a vehicle will be protected by vehicle reducing the dose. When the RPF value falls below 1, dose inside of a vehicle will be higher than the dose received from outside of the vehicle, meaning the vehicle will no longer protect the person. Although current estimates of RPF [5-7] values have been conducted for simplified geometries, the most efficient way to acquire RPF for vehicles is to validate the computational models. In the realm of defense, accurate and verifiable RPF values of military vehicles will correctly inform commanders and strategic decision-makers of optimal force employment and risk management on a nuclear battlefield [5].

Due to using simplified models, these codes are quite efficient in terms of time and resources. Thus, the need exists to validate the simplified mathematical models used in

code with developed computational models such as the human phantom, radioactive material transport package, and contaminated environments. This increases the reliability of the codes ensuring public that these values are sufficient to estimate the actual dose value. The proposed way to approach this concern is to indicate potential radiological consequences from the package is in incident-free transportation and hypothetical incident conditions where radioactive material spills on the road, and radioactivity released from the radionuclides contaminates the environment. Furthermore, previous literature [5-7] has performed RPF analyses for simplified vehicle geometries and well-defined radiation fields utilizing monoenergetic photon and neutron sources comparing to high-yield, short-duration prompt neutron and photon spectra from a fission weapon. Thus, there is a need for more realistic vehicle models considering the different parts and shapes of vehicles surrounded by radiological contamination dispersed in the air (cloudshine) and on the soil (groundshine), as in a field of radiation being produced from the decay of radionuclides on the ground or in the air in the event of environmental contamination.

The approach to improve the RPF for vehicles in an incident resulting in environmental contamination is to augment current approaches using simple calculations and models with developed, state-of-the-art computational capabilities. Analyses can be made using more realistic vehicle models instead of a simple steel box, computational phantoms instead of prior approaches using an ICRU sphere [8], and proper environmental exposure scenarios that represent the contamination resulted from transportation accidents or radiological dispersion. This can result in increasing the effectiveness reliability of RPF

for vehicles, which in return also creates a more computationally efficient model for emergency preparedness and consequence management.

2. BACKGROUND

2.1. Dose Calculations

Due to the importance of radiological protection in the transportation of radioactive materials, radiation measurements, such as exposure and dose quantities, play a vital role in transportation safety, nuclear/radiological preparedness and consequence management protection regulation. In the latest recommendations by the International Commission on Radiological Protection (ICRP) in Publication 103 [9], a recommendation for the calculation of radiation protection quantities is defined. The essential quantity for limiting objectives in radiation protection is effective dose, E (Sv). There are a few important quantities to note in order to compute the effective dose, which serves as the foundational quantity on which radiation protection regulation for occupational workers and members of the public is derived. The first quantity is absorbed dose (Gy), which is defined as a fundamental and measurable dose quantity, which is the mean of the stochastically distributed energy deposition in a volume element [9]. In essence, absorbed dose is the energy absorbed from any type of radiation per unit mass and is deemed to be an acceptable measurement of chemical or physical effects from radiation exposure. Consequentially, the ICRP [10] introduces the derived quantity of equivalent dose, H_T (Sv), and is computed by absorbed dose averaged over the specified tissue and organs using a dimensionless radiation weighting factor (w_R) and considers the differences in sensitivity of specified tissue and organs, as defined in Equation 2:

$$H_T = \sum_R w_R D_{T,R} \qquad Eq. 2$$

where $D_{T,R}$ is the average absorbed dose in a specified tissue or organ T and radiation type R, as shown in Table 1 with corresponding weighting factors as defined in ICRP Publication 103 [10].

Table 1. Radiation weighting factor values for different radiation types.

Radiation Type	**Radiation weighting factor, w_R**
Photons	1
Electrons and muons	1
Protons and charged pions	2
Alpha particles, fission fragments, heavy ions	20

Tissue weighting factor (w_T) is defined as sex- and age-independent radio-sensitivity of specified tissue or organ by the ICRP. The values of w_T are shown in Table 2 and the sum of all the tissue weighting factors is equal to 1 [9, 10]. Effective dose is a sex-averaged quantity, necessitating consideration of both male and female exposure models in the computation of the derived quantities of equivalent and effective dose. Equivalent dose can be weighted for corresponding values of tissue weighting factors regarding the type of tissue, and is summed to find the effective dose in units Sievert (Sv) by Equation 3:

$$E = \sum_T w_T \left[\frac{H_T^M + H_T^F}{2}\right] \qquad Eq.3$$

where H_T^M and H_T^F represent the equivalent dose to tissue of the male and female phantom, respectively.

Table 2. Tissue weighting factors for organ and tissues.

Tissue	w_T	$\sum w_T$
Bone marrow, breast, colon, lung, stomach, remainder tissues*	0.12	0.72
Gonads	0.08	0.08
Urinary bladder, esophagus, liver, thyroid	0.04	0.16
Bone surface, brain, salivary glands, skin	0.01	0.04

*Tissue weighting factor is 0.00923 for remainder tissues: adrenals, extrathoracic (ET) regions of the respiratory tract, gall bladder, heart, kidneys, lymphatic nodes, muscle, oral mucosa, pancreas, small intestine, spleen, and thymus except for uterus/cervix (female) and prostate (male) which is 0.00462.

Effective dose has been determined to be a foundational quantity by the ICRP for radiation protection; however, it cannot be directly assessed experimentally due to application of tissue weighting factors being biological quantities and not physical quantities. With the limitations for effective dose studies, this presents the need for computational analyses by making use of the environmental impact and risk assessment codes in RAM transportation analysis.

2.2. Computational Phantoms

When performing computational analyses for the aforementioned effective dose, one consideration is computational phantom models. Computational phantom models

such as the Oak Ridge National Laboratory-University of Florida (ORNL-UF) stylized phantom model [11] have previously been simplified in the vertical-upright position with arms attached to the torso and rigid legs. Stylized phantoms basically illustrate the human body mathematically considering the characteristics of organs such as the volume, density, location, and the shape of various organs. However, in previous literature [12], it has been demonstrated that there is a high variability for organ doses for receptors in articulated positions compared to the simplified upright phantom model [13]. This high variability led to the need of the Phantom with Movable Arms and Legs (PIMAL) software developed at ORNL, which is a computational phantom with moving arms and legs [14]. PIMAL development has proven that a computational model of human anatomy, or a phantom, has gone through many iterations since development began in the 1970s [15]. The PIMAL software has numerous capabilities such as the possibility to assign posture to male and female phantoms, which in result generates a corresponding input deck for the Monte Carlo N-Particle (MCNP) transport code [16]. The PIMAL mathematical male and female phantoms can be articulated in a sitting or working position in any type of vehicle or environment by making proper adjustments in the input provided by the PIMAL. This is a unique capability developed at ORNL, as other standard models are only capable of modeling persons in a straight standing posture and represents a greater accuracy when modeling computational phantoms [12, 17]. The stylized phantom was selected compared to other available phantom models, as it was demonstrated in prior work by Bellamy et al.[18] and Hiller and Dewji [19] that voxel (CT-based) phantom models yielded comparable organ and effective doses as stylized, in environmental contamination

scenarios, with the exception of thin-walled organs (e.g., esophagus, skin, small intestine) or at low energies as a result of differences in organ depth distributions in the phantom explained in Griffin et al.[20] Furthermore, the PIMAL stylized phantoms permitted manipulation into an operating posture in a transportation vehicle.

It should be noted that per the ICRP Publication 103 definition, effective dose is meant to serve as a protection quantity for prospective dose assessment for radiation protection planning to demonstrate compliance within regulatory limits, but not for epidemiological evaluations or individual retrospective investigation [9]. The methodology reported here does calculate effective dose for articulated postures to provide a relative comparison of detriment vis-à-vis the estimation of traditionally reported fluence-to-dose in an upright posture. Therefore, for purposes of individual dose estimation or reconstruction, specific organ doses derived in this work should be consulted.

2.3. Transportation Dose Limit and Transport Index

The transport index (TI), is a dimensionless parameter on the label of a radioactive material package and is an indication to determine the external radiation of an undamaged package. Referring to Figure 1, the value in the lower right corner shown is the TI can be a starting point for determining whether a damage has occurred or not. It is an essential quantity to show the degree of control to be exercised by the handlers during transportation. The TI is equal to the highest radiation level in mrem/h (where 1 mrem = 0.01 mSv) at 1 m from an undamaged package. A distinction is made between shipments

under exclusive and non-exclusive use, as well as dose limits are set for transportation packages by the transportation regulations. According to the NRC Title 10 of the Code of Federal Regulations (10 CFR) [21], the dose of a transportation package at any point on the external surface and at 1 m from the external surface should not exceed 2 mSv/h, and 0.1 mSv/h, respectively. When transportation is classified under exclusive use, the radiation level at any point on the external surface of the transportation package should not exceed 10 mSv/h. Furthermore, the reference value of lifesaving or protection of large populations for emergency responder radiation safety is provided by the National Council on Radiation Protection and Measurements (NCRP) Report 179 as 250 mSv.[22]

Figure 1. A radioactive material package label.

2.4. RADTRAN Transport Risk Analysis Code

Since the initial release of RADTRAD in 1977, continuous development of the RAM transportation models in RADTRAN remains. The capabilities of the risk and consequence analysis code were continued with the subsequent releases of RADTRAN II in 1983 [23], and RADTRAN III in 1986 [24]. Until the release of RADTRAN 4 [25] in 1992. The code lacked route-segment-specific values such as population density, vehicle

speed, and traffic count which allowed for route-specific analyses of RAM transportation. RADTRAN 5 released in 2000 [1] continued to allow for more realistic simulations such as accident-free RAM transportation. This brings development progress to the current Nuclear Regulatory Commission (NRC) RADTRAN code, 6.02.01 [26].

Currently, RADTRAN is a risk and consequence analysis code that allows for quantifying estimates of the transportation of radioactive materials with numerical models of exposure pathways, receptor populations, package behavior in accidents, and accident severity and probability [26]. RADTRAN is a unique environmental impact and risk assessment code for analysis of transportation of radioactive and other hazardous materials. This risk analysis code estimates consequences and risks associated with routine, incident-free transportation of radioactive materials and with incidents that might occur during RAM transportation. An essential input parameter for RADTRAN simulations is the previously discussed TI value for all types of packages however the radionuclide inventory data are not essential for incident-free dose calculation.

Since RADTRAN includes mathematical models for both stationary and transient models, radiation doses from incident free transportation may be calculated for any desired groups of workers and members of the public, such as: vehicle crew members, cargo handlers and inspectors, warehouse personnel, as well as passengers. However, dose to handlers and inspectors are special types of calculations since small populations may come near to the RAM vehicle. Hence, the number of handlers and/or inspectors, as well as their distances from the RAM shipment are additional required inputs for these calculations and

the stationary dose model is applied, which is based on point and line source models regarding the radial distance from the source and the package dimensions.

For small packages, dose rate is inversely proportional to the square of the radial distance from the source at distances large compared to the package dimensions. It was found that a point-source model yields dose rates that are slightly larger than the actual dose rates measured at distances between the source and the receptor greater than the critical package dimension (CPD) [27]. The point source formulation for different shaped packages, and the CPD, is shown in Figure 2. For a cylindrical package, the CPD would be either the axis of the cylinder or the diameter, whichever is larger. For larger packages, a line-source model is used at distances less than twice the critical package dimension. Dose rate and distance from the source are inversely proportional to each other along the entire length of the source (Figure 2). Although RADTRAN can result in larger values, the use of the RAM transportation code can provide reasonable results for several analyses without extensive computational resources [26].

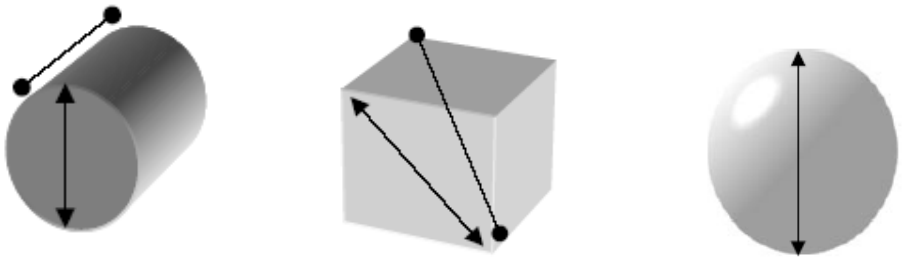

Figure 2. Critical dimension of the transportation package used in RADTRAN.

The gamma dose-rate for an isotropic point-source is basically determined in the RADTRAN code as shown in Equation 4:

$$DR_{\gamma}(r) = \frac{S_{photon}}{4\pi r^2} \text{ x } e^{-\mu r} \text{ x } B(\mu r) \qquad Eq.4$$

where $DR_{\gamma}(r)$ represents the gamma dose rate in mrem per hour at radial distance r in meter, S_{photon} represents the photon emission rate in photons per second. Incident-free population dose from external radiation emitted by RAM packages is utilized in most cases using an expression for dose rate as a function of distance from an isotropic point source which emits radiation with equal magnitude in all directions [4]. In this approach, the highest dose rate value taken from the 1 m away from the package surface is equal to the radiation field strength from the isotropic point source at a distance of 1 m plus the half of the critical package dimension CPD, as shown in Equation 5:

$$DR_i(r) = f_i \text{ x } DR_{PKG} \text{ x } e^{-\mu_i r} \text{ x } B_i(r) \left[\frac{(1 + 0.5d_e)}{r}\right]^m \qquad Eq.5$$

where

i = Index variable (γ for gamma, n for neutron radiation)

r = Distance between source and receptor (m)

$DR_i(r)$ = Dose rate as a function of distance (mrem/h)

DR_{PKG} = Dose rate of package at 1 m from the package surface (mrem/h)

f_i = Fraction of the radiation field of gamma or neutron

μ_i = Attenuation coefficient of gamma or neutron in air (m^{-1})

$B_i(r) =$ Build-up factor for surrounding medium at distance r

$d_e =$ Effective package dimension (m) (CPD for packages ≤ 4 m)

m = 1 when r < d_e or 2 when r ≥ $2d_e$

Several articles discuss experimental measurements used to validate the transient dose model used to estimate the dose to an individual when radioactive material package passes the stationary individual. One of the experiments were performed by Steinman et al. [27] using a well logging calibration source containing 1.85 GBq ^{241}Am and 0.37 GBq ^{137}Cs in a DOT 7A, Type A package. Dose data were taken at 1 and 3 m distances from the edge of Albany Avenue as the truck drove past the stationary detectors with 8 and 16 km/h speeds [27]. Depending on the type of the radiation field, the neutron component or the gamma component can be ignored and since only the gamma radiation is considered here, then the Equation 5 is simplified into:

$$D_\gamma(r) = \frac{k_o \text{ x } DR_{PKG} \text{ x } e^{-\mu_i r} \text{ x } B_\gamma(r)}{r^2} \qquad Eq.6$$

where $D_\gamma(r)$ represents the dose to a person from one shipment of gamma emitting material and k_o is the package shape factor which equals to $(1 + 0.5d_e)^2$. When integrating Equation 6 from -∞ to ∞ with respect to time which is given by Equation 7, where v represents the speed of vehicle, x represents the distance of closest approach between the package and the receptor:

$$D_\gamma(x) = \frac{2 \text{ x } k_o \text{x } DR_{PKG}}{v} \int_x^\infty \frac{e^{-\mu_i r} \text{ x } B_i(r)}{r\sqrt{r^2 - x^2}} dr \qquad Eq.7$$

Since the important gamma radiation energy interval is 0.4-0.9 MeV and the product of gamma attenuation and build-up in air is usually less than 1[28], the RADTRAN model assumes the product of gamma attenuation and build-up in air is equal to 1, which reduces the integral to a form that has an analytic solution [1]:

$$D_\gamma(x) = \frac{k_o \text{x } \pi \text{ x } DR_{PKG}}{vx} \qquad Eq. 8$$

The study demonstrates that the RADTRAN model over predicts the measured dose within an order of magnitude of the measured integrated individual dose value employing Equation 8. The study displays that at distances more typical of residential populations alongside the road, the RADTRAN model provides better agreement with the actual experienced doses [27].

2.5. Radiation Protection Factor for Vehicle

As the value of RPF increases, the larger the dose reduction due to shielding provided by the vehicle. The assessment of RPF also reports information about optimal positioning of the vehicle, which is relative to the location of radiation source, in order to decrease the radiation exposure to individuals. Thus, in military applications, assessment of RPF values for vehicle plays a vital role in risk assessment and mission planning when working in radiation environment.

In a previous study, Burson [29] focused on evaluation of environmental and fallout gamma radiation protection factors for several civilian transportation vehicles using measurements of the natural terrestrial radiation as a source. The pulse-height spectrum is investigated for vehicles to indicate if there is any sources of radiation in the vehicle. The protection factors range was found as 1.7 to 3.5 which are applicable for fallout radiation or for natural terrestrial radiation by comparing free-field spectra with spectra observed inside vehicles [29]. This study emphasizes the environmental RPF provided by several positions in civilian vehicles but is given for a constrained set of experiment-based data, and sources outside of the vehicle were not addressed.

McHale et al. [6] focuses on estimating RPF values for a simple surrogate vehicle using MCNP6.1 for 25 photon energies and 53 neutron energies. RPF values for military and civilian vehicles are obtained using a surrogate vehicle (steel cube) which has 60.96 cm side length and 1 inch wall thickness, in keeping with historical and recent studies estimating the energy-dependent absorbed dose at a 10-mm depth in the 30-cm-diameter ICRU tissue equivalent sphere [8]. The radiation field is tallied for photon and neutron then converted to fluence-to-ambient dose equivalent conversion coefficients. The study stated that while the protection of steel cube is good for lower photon energies with high RPF values, for energies 2.0 MeV and greater the RPF values approaches about 1.4, and for all energies, the ambient dose equivalent would not be higher than about 1/1.4, or about 70% [6]. The approach to RPF for current U.S. military vehicles is to provide a reliable and cost-efficient method by emphasizing the importance of computational effort.

Nevertheless, this article is successful about using the fluence-to-ambient dose equivalent conversion coefficients to estimate the MCNP6.1-computed and experimentally-validated RPF values, which are for simplified vehicle geometry and well-defined radiation field utilizing monoenergetic photon and neutron sources comparing to high-yield, short-duration fission neutron and photon spectra from a fission weapon instead of dispersed environmental contamination from dispersal/accident, and the results cannot be extended directly to contaminated environment scenarios [6].

Takahara et al. [30] discussed the dose reduction factors of vehicles developed based on weight and actual geometry of Japanese vehicles. Although the actual shape of the vehicles was not rectangular, vehicles were assumed as rectangular shape not considering any slope with the windows located on four sides of the vehicle. However, the thicknesses of the vehicles used in the simulations were 0.70 cm, 0.78 cm, 0.86 cm, and 0.93 cm, comparisons were done using the weight of each vehicle increasing with the thickness of the vehicles. Dose reduction factor is calculated as the ratio of ambient equivalent dose rate taken from inside of the vehicle to which from outside of the vehicle, which is the inversed version of RPF. Photon flux is calculated using point detectors and then converted employing the ICRP Publication 74 [31]. This study also compares the modeled calculations with actual measurements taken from the area contaminated by the Fukushima Daiichi Nuclear Power Plant (NPP) accident after 55 months. Thus, the radionuclides with short life decreased and the most contributing radionuclides were ^{134}Cs and ^{137}Cs. Experimental measurements were performed using a NaI(Tl) scintillation

survey meter in Futaba Town in Fukushima prefecture where a pilot decontamination was conducted about 2 years ago from the experiment.

Although the dose reduction factors of vehicles for cloudshine (air contamination) are obtained for photons with 0.4, 1, and 1.5 MeV energies, which for groundshine (soil contamination) are evaluated for only ^{137}Cs source concentrated at a depth of 0 to 10 g cm^{-2} in soil. Tables 3 and 4 show the dose reduction factors of vehicle models converted into RPF form of Takahara et al.'s work for cloudshine and groundshine, respectively.

Table 3. Dose reduction factors of vehicle converted into RPF for cloudshine for various photon energies.

Thickness of vehicle (cm)	0.4 MeV	1 MeV	1.5 MeV
0.70	1.37	1.18	1.14
0.78	1.39	1.19	1.15
0.86	1.41	1.20	1.16
0.93	1.51	1.28	1.22

Table 4. Dose reduction factors of vehicle converted into RPF for groundshine for various relaxation mass depths considering only the contribution of ^{137}Cs.

Thickness of vehicle (cm)	0 g cm^{-2}	5 g cm^{-2}
0.70	1.37	1.45
0.78	1.37	1.51
0.86	1.51	1.56
0.93	1.56	1.67

The experiment is performed under the assumption of that only ^{137}Cs is located on the ground surface for groundshine calculations and cannot be easily extended to protection factors of every radionuclide of concern in the soil contaminated environment.

Furthermore, the vehicle data is sourced by a Japanese automaker which is not easily accessible information and even if the vehicles are based on the actual size and thickness of Japanese vehicles, they are modeled still in a rectangular shape. However, the study showed that the dose reduction factor of a 0.9 cm-thick-vehicle for groundshine is 0.64, meaning the RPF representation is 1.56, for ^{137}Cs source concentrated at a depth of 0 g cm^{-2} in soil, experimental data is ranged from 0.54 to 0.65, resulting in an RPF from 1.85 to 1.54.

2.6. Environmental Contamination

The previous studies suggested a pathway to calculate effective dose rate coefficients for external photon exposure to photons emitted by radionuclides distributed in air and soil, respectively [18, 32]. These data were summarized in the Environmental Protection Agency's Federal Guidance Report (FGR) No. 15, *External Exposure to Radionuclides in Air, Water and Soil* [33], which provides information for use in executing radiation protection programs and FGR 15 is updated version of Federal Guidance Report No. 12, *External Exposure to Radionuclides in Air, Water, and Soil* [34]. This report tabulates age-specific, reference person effective dose rate coefficients for 1,252 radionuclides based on external exposure to radionuclides distributed in air (i.e., cloudshine), water and soil (i.e., groundshine) [33]. Federal Guidance Report No. 15 includes up-to-date scientific knowledge for regulation of radiation exposure for indicating the relationship between radionuclide concentrations exists in the environment and the dose to members of the public from environmental radiation exposure. While

environmental exposure rate is calculated assuming monoenergetic infinite planar sources are located at 3 mm for soil contamination which is then normalized to unit strength in 1 Bq m^{-2}, exposure rate from submersion in contaminated air (cloudshine) scenario is evaluated assuming monoenergetic photons in a semi-finite cloud are uniformly distributed with 1 Bq m^{-3} surrounding a phantom standing on the air-ground interface. Afterward, the coefficients are interpolated using a log-linear Hermite cubic spline [35] and then integrated into numerical values. However, these studies [18, 32-34] play an essential role in estimating dose rate coefficients for semi-idealized environments, it does not take into account vehicle shielding materials and phantom posture inside of the vehicle, and thus has limited utility in RAM transportation calculations.

3. OBJECTIVE

The purpose of this work was to provide a generic assessment of the effective dose received by individual due to the RAM package under both incident-free and hypothetical incident condition of transport to address public concerns about the safety of the transportation system. This assessment will include the following two investigatory tasks:

1. Comparison of RADTRAN models for incident-free transportation validating with Monte Carlo simulations; and

2. Tabulating gamma RPF of the model vehicle for male and female mathematical phantoms on the driver seat, from external exposure to photons emitted by radionuclides distributed in air, soil, and inside of a truck-trailer.

The first task compared RADTRAN estimates the dose as to the dose from the actual package model by evaluating the models used in the code. This was conducted using Monte Carlo radiation transport simulations to compute exposure dose to individual male and female mathematical phantoms at several distances between package and the receptor resulting from RAM package. The second task estimated doses from incident scenarios modeled in the first task, resulting in soil contamination (groundshine), air contamination (cloudshine), and truck-trailer contamination using realistic models of transportation vehicles and operators within and exterior to the RAM. An analysis of the simplified mathematical models used in transportation risk code for incident-free transportation and the radiation protection factor values for vehicles under hypothetical incident condition of

transport provided a comparison to the established RADTRAN transport code and the effectiveness of RPF values for vehicle.

4. METHODOLOGY

4.1. Incident-free Condition of Transport

The incident-free scenario was created considering the external radiation to workers when the package was being loaded to a vehicle by workers, or when the transportation mode changes (truck to rail, truck to air, etc.). Consequently, workers need to interact with the packages more likely and spend more time near the packages. Evaluation of the incident-free condition of transport was started modeling a Type A package used in one of the experiments explained by the previous study [27]. Afterwards, computational male and female phantoms which represented the worker, were placed at various locations, ranging from 0.1 m to 10 m, near the package to determine the dose rate as shown in Figure 3. The corresponding scenario is called “Handling” in RADTRAN transportation code and it is under the stationary dose model. Since this model is based on the point and line source approximation, the same scenario was also simulated replacing the package with simplified point and line source depending on the relation between distance to worker and critical package dimension. Throughout this study, only gamma-ray emitting sources with uniformly distributed activity from radionuclides were considered and PIMAL mathematical male and female phantoms were used.

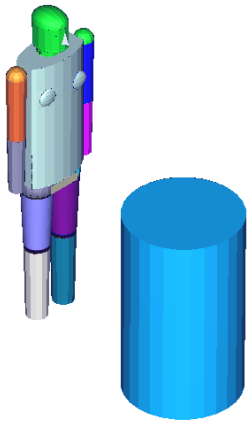

Figure 3. Modeled package and a phantom used in incident-free simulations.

4.1.1. Type A Package

One of the basic types of packaging, Type A package, mostly involves steel drums used in waste storage, transportation, and disposal [36] which must meet the requirements of US Department of Transportation specification 7A (DOT-7A) of the 49 CFR [37]. A Type A package was modeled using MCNP6 in order to be used in the next section. The TI value, source term, and dimensions of the package were the main considerations in the design process. The thickness of the package was determined locating the MCNP6 (F5Z:P tally) ring detector at 1 meter outside of the package surface since the TI value is the dose rate at 1 meter outside of the package surface. The characteristics of the modeled package are shown in Table 5.

Table 5. Modeled Type A package parameters.

Package Content (isotope)	Well logging calibration source (1.85 GBq ^{241}Am and 0.37 GBq ^{137}Cs)
TI (mrem/h)	1.2
Critical Package Dimension (CPD) (m)	1
Length (m)	1
Radius (m)	0.3
Material	Stainless Steel

4.1.2. RADTRAN Analysis

For the stationary dose model, the program's GUI was used defining the package parameters shown in Table 3 and the handling parameter which was the distances between the package and the handler. The scenario was created in RADTRAN transport code and the dose results were taken for handlers as it represented the stationary dose model. Since the stationary dose model calculations differ by line and point source model regarding the relation between package size and package-to-receptor distance, the stationary dose model was evaluated simulating the same line and point source model around phantoms in MCNP6. The important point to be considered when modeling the point-line source version of an actual package was that RADTRAN takes the distance between receptor-to-source from the geometrical center of the package instead of the package surface. The TI value was extrapolated back to the center of the package to achieve the source definition used in the MCNP simulations. The changes in the intensity of the external radiation were unchanged regarding simplification of this extrapolation, then the TI value were employed

to describe the radiation field strength at various source-to-receptor distances from the package center to package dimension plus 1 m. The shape of the actual package was converted into an equivalent spherical volume. RADTRAN output file indicated which radial distance would be treated as point or line source model and according to this MCNP simulations were created. Line source model was also simulated with the same manner considering the source was along with the critical package dimension. To calculate the potential dose to members of the public and to the workers resulted from a Type A package in the incident-free transportation scenario, a kerma approximation (F6) tally was used to tally organ absorbed dose from photon deposition at various distances, ranging from 0.1 m to 10 m, between the package and a standing phantom will be taken using phantoms and the representative model of the package in the three-dimensional Monte Carlo N-Particle transport code, MCNP6 [16] (Figure 3). Tallied organ absorbed dose data were then converted to effective dose value employing ICRP Publication 103 recommendations [10].

4.2. Hypothetical Incident Condition of Transport

The hypothetical incident scenario was created assuming radioactive material spills on road and radioactivity released in the air from the radionuclides. Calculation of radiation protection factor for vehicles in a contaminated environment were simulated using different representative vehicle models which consist of 1-cm steel box, 1-inch (2.54 cm) steel box, and a more realistic vehicle. Vehicle model was developed based on either the actual shape of a vehicle, including sloped window, representative engine, and the

main body. Computational male and female phantoms, representative of the driver (Figure A-1), were placed inside of each vehicle as in driving position and on driver seat location. However, contaminated external exposure scenario consisted of soil contamination and air contamination, as conducted with FGR 15, this study was also extended to the scenario with contamination inside of a truck-trailer. Tissue and organ-specific dose rate coefficients were computed in mathematical phantoms representing male and female for monoenergetic photon sources at 17 discrete energies, ranging from 0.04 to 3 MeV. An energy cutoff of 0.04 MeV was identified based on preliminary simulations as yielding optimal convergence statistics in the Monte Carlo run in the presence of shielding material between the environmental source and receptor in the vehicle.

Photons calculations for contaminated scenarios are described as two steps using surface source write (SSW) and surface source read (SSR) feature in MCNP [18, 32, 33, 38]. For the first step (SSW), a coupling surface were chosen to be large enough considering the vehicle, given in Figure 5. The incident photons were be recorded on the coupling surface using SSW feature and then the recorded incident photons on the coupling surface were used for the second step which the phantom and vehicle is located inside as the source definition using SSR feature (Figure 5). All these steps were repeated for 17 discrete energies, for male and female, and for different vehicle models, as well as contaminated scenarios. While unshielded dose was taken in the first step when the vehicle and phantom models are not inside of the coupling surface using F6 photon tally, the shielded dose was taken in the next step where the vehicle and phantom is located inside of the coupling surface to estimate RPF values for the modeled vehicles in a contaminated

environment. It was assumed that only monoenergetic photons as a preliminary indicator of RPF and the occurrence of the bremsstrahlung effect was not explored in the scope of this work.

4.2.1. Vehicle Models

The calculation of the shielded dose in each of the contaminated environment scenario was performed using 3 different representative vehicle models. First, a 1-inch thickness simple steel box was modeled in order to keep up with the previous work however the dimensions of the simple box were altered to be able fit the phantom inside of the box as shown in Figure A-2. For the second vehicle model, the thickness of the same box was changed to 1 cm to observe the effect of thickness on RPF. Finally, the more realistic vehicle model which consists of carbon steel and fiber glass material (Table A-1) were modeled based on the actual shape of a vehicle, including a sloped window, a representative engine, and the main body (Figure A-3). The three aforementioned designs are created using Computer Assisted Design (CAD) models; however, they lack information to export point coordinates to create MCNP surface input cards. The CAD models for larger structures, such as the vehicle models, are often referred to as the Boundary Representative (BREP) structures, but they need to be converted using software to adapt for MCNP geometry. By making use of Rhinoceros [39], a commercial 3D computer graphics software, with the visual scripting language add-on, Grasshopper (GH), the BREP CAD structures can be converted to the necessary points for MCNP surface cards [40]. Because of the complexity of the vehicle, only 1 cm depth was included for

this model considering the variance reduction techniques were applied and the difficulty for the lower photon energies. The dimensions of the vehicle models are shown in Figures A-2 and A-3.

4.2.2. Contaminated Scenario Calculations

Photon calculations for contaminated scenarios were described as two steps using SSW and SSR feature in MCNP [18, 32, 33, 38]. For the first step (SSW), a coupling surface was chosen large enough considering the vehicle, given in Figure 4. The incident photons were recorded on the coupling surface using surface source write feature and then the recorded incident photons on the coupling surface were used as the source definition using surface source read feature for the second step which the phantom and vehicle is located inside of the coupling surface (Figure 5). All these steps were repeated for 17 discrete energies ranging from 0.04 to 3 MeV, for male and female phantoms as well as for different vehicle models. The calculation of effective dose rate for mathematical male and female phantoms were performed employing the tissue weighting factors recommended in ICRP Publication 103. While unshielded dose was taken when the vehicle was not present inside of the coupling surface, the shielded dose was taken when the vehicle and phantom were located inside of the coupling surface to estimate RPF values for the modeled vehicles in various contaminated environments. The summary of the details used in contaminated environment simulations can be found in the Table 6.

Table 6. Details of method used for contaminated environment simulations.

Radiation transport (code)	Monte Carlo (MCNP6)
Phantom library	Mathematical male and female (PIMAL)
Tissue weighting factors	ICRP Publication 103
Radiation considered	Photons
Decay data	ICRP Publication 107
Soil profile	An infinite planar source uniformly concentrated at a dept of 0.5 g cm^{-2}, which is equal to 1.6 x 10^3 kg m^{-3} soil for 3 mm
Air profile	Semi-infinite uniformly concentrated air cloud in a side length of 10 m cube
Monoenergetic interpolation grid	17 energies
Variance reduction	Path-length stretching, reflective boundary condition
Variance reduction for vehicle	Geometry splitting, weight window

4.2.2.1. Soil Contamination

4.2.2.1.1. Geometry Overview

Calculation of contaminated soil scenario was performed assuming monoenergetic infinite planar photon sources which are located at 3 mm depth in the soil normalized to 1 Bq m^{-2} source strength and emitted in an isotropic behavior. The result of these planar sources in the soil was recorded on a coupling cylinder of height 230 cm and radius 170

cm and were then used to calculate the tissue dose coefficients for a phantom in a driving position inside of a vehicle as shown in Figure 5. The elevation of the air above the soil was assumed as 3 mean free paths (mfp) depending on the source energy. When photons scatter at a height higher than 3 mfp in the air, they would travel more than 6 mfp from the source to reach the coupling cylinder and, thus, there would not be a notable contribution to tissue dose. The phantom and the vehicle were not included in geometry description to remove the complexity of the human phantom as well as the vehicle for the calculation of the incident radiation field. However, this can be performed if the incoming angular flow rate on the coupling surface is not perturbed by the phantom, it is established by Saito et al. [41] that the phantom has a significant effect (up to a second-order effect) on the incoming directions of photons which have an interaction in the phantom by scattering in the surrounding environment and returning back to the coupling surface.

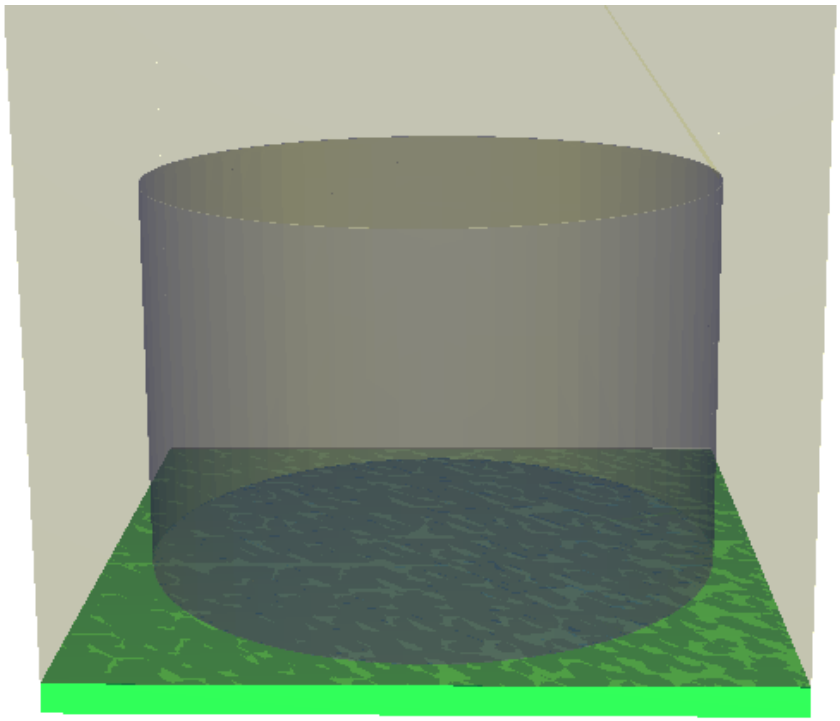

Figure 4. Cylinder used in SSW step representing the coupling surface for soil contamination.

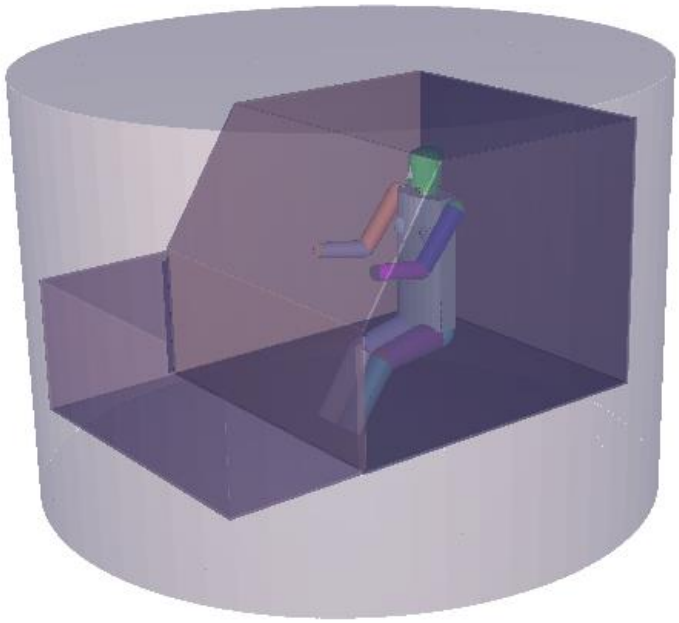

Figure 5. The vehicle model with phantom inside of the coupling surface used in SSR step.

4.2.2.1.2. Soil Composition and Ground Characteristics

The soil composition used in this work is shown in Table 7. This typical silty soil [42] composition was containing 30 percent water and 20 percent air by volume and its density was assumed as 1.6 x 10^3 kg m^{-3} to be consisted with the previous works. The monoenergetic infinite planar photon sources were at a depth of 0.5 g cm^{-2}, which is equal to 3 mm for a soil density of 1.6 x 10^3 kg m^{-3} in order to consider the ground roughness. The thickness of the half-space of soil was assumed as 3 mfp depending on the source energy. The radiation field resulted from the isotropic infinite plane sources was determined for 17 discrete energy and the air-ground interface was idealized as a flat plane with no soil covering the radioactivity, other than accounting for ground roughness.

Table 7. Soil composition.

Element	Mass Fraction
H	0.021
C	0.016
O	0.577
Al	0.05
Si	0.271
K	0.013
Ca	0.041
Fe	0.011

4.2.2.1.3. Photons and Dose Calculations

As discussed prior, the photon calculations were divided into two steps. In the first step, the calculation of incident photons on the coupling cylinder surface was achieved without involving the phantom as well as the vehicle models. A cylinder of height 230 cm and radius 170 cm was employed to act for coupling surface for the SSR step. This cylinder was chosen to be as small as possible to ensure efficient recording to the coupling source but large enough to enclose the largest vehicle model. The distance between the coupling cylinder and the air-soil interface was assumed as 0.1 cm. The photon transport was not affected by the existence of the coupling cylinder since it would act as a passive detector/recorder of the photons. The source particles located at the 3 mm depth of soil were created throughout the ground plane. The incident photons calculations on the coupling cylinder surface were completed using SSW feature in Monte Carlo transport code MCNP6. By using SSW feature, energy, position, and direction vector of the uncollided and scattered photons from isotropic plane sources were recorded. The recorded incident photons in the SSW step were then used for the SSR step, which including the phantom inside of a vehicle in order to be used for shielded dose calculations. In this step, the inside of the coupling cylinder volume was filled with air.

The next step for photon calculations was to determine the dose rate coefficients in male and female mathematical phantom using the recorded photons from the first step. This recorded incident photons were employed as source definition using the surface source read feature in MCNP. In this step, each phantom was located inside of each vehicle model separately. The volume between the phantom and the coupling cylinder were filled

with air, as well. For all photon transport calculations, tissue kerma approximation was assumed and the tissue dose rate calculations were performed using photon fluence and tissue-specific kerma coefficients. The photon fluence was generated using average track-length estimator (F6:P tally) in MCNP transport code. Organ dose rate coefficients were computed for 17 discrete photon energies, three vehicle models, and two phantoms. Afterwards, calculation of the effective dose rate coefficient was performed using tissue weighting factors as recommended in ICRP Publication 103.

4.2.2.2. Air Contamination

4.2.2.2.1. Geometry Overview

Air submersion scenario was created assuming a phantom in driving position inside of a vehicle and exposed to a uniform air contamination of monoenergetic photon emitter. This scenario was assumed as a semi-infinite air cloud source and the dose from a semi-infinite cloud source near the air-ground interface was taken as half the dose from the infinite cloud source according to the previous work [43-46]. This method has been proven as to be a good approach for the energies 20 keV and higher by Ryman et al.[46]. However, the computational method of air contamination was including the same 2 steps explained in the soil contamination calculations, computational geometry shows differences. The phantom and the vehicle were not included in geometry description to remove the complexity of the human phantom as well as the vehicle for the calculation of the incident radiation field. Calculation of submersion in contaminated air scenario was performed assuming uniformly distributed monoenergetic photon in a semi-finite air cloud

with 1 Bq m^{-3} in a side length of 10 m cube (Figure 6). The coupling cylinder was located at the middle of the air cube. The six walls of the cube were simulated as reflectors in MCNP so that the energy of particles was conserved.

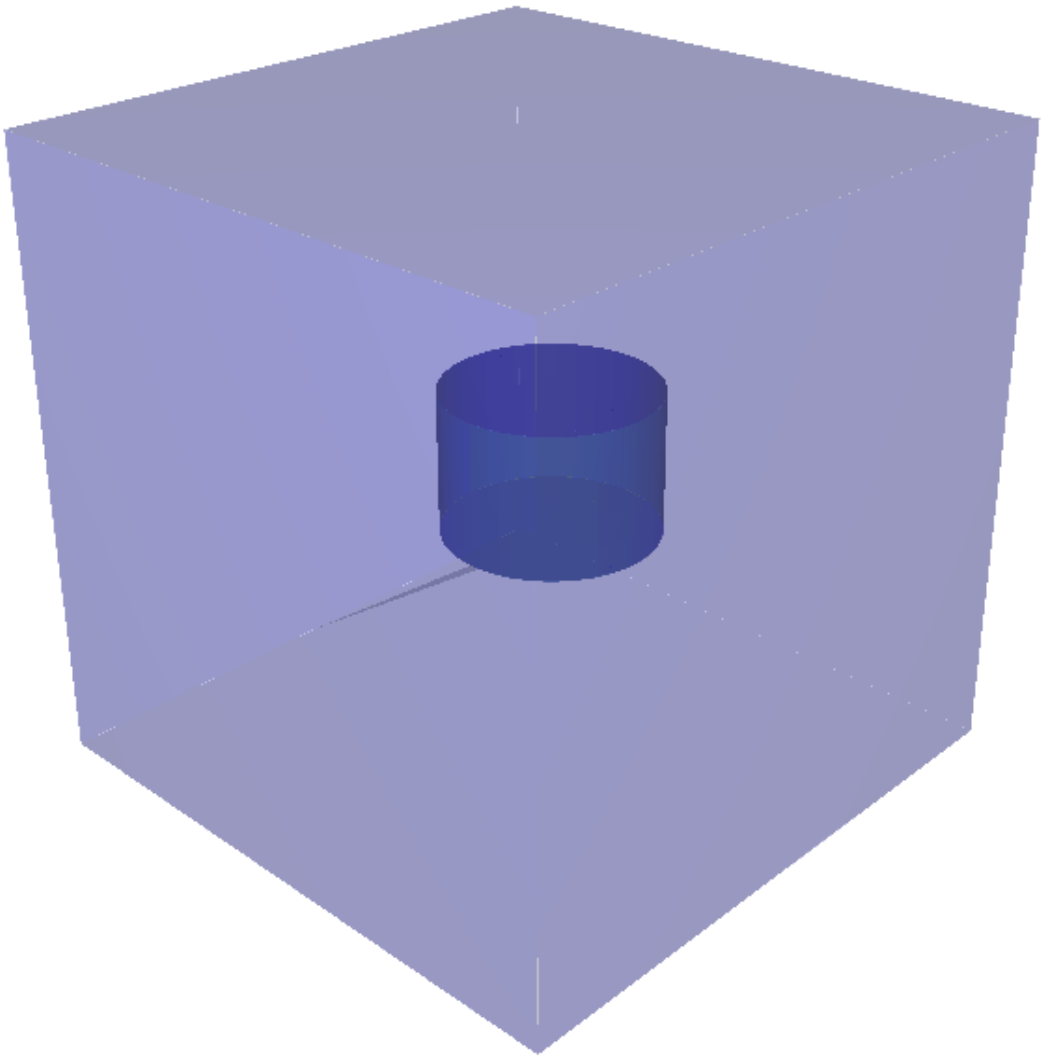

Figure 6. Cylinder and air cube used in SSW step for air contamination.

4.2.2.2.2. Air Composition

The air composition used in this work is shown in Table 8. This air composition represented here was for 40 percent relative humidity, 760 mmHg pressure, and 20 ºC temperature and its density was assumed as 1.2 kg m^{-3}.

Table 8. Air composition.

Element	Mass Fraction
H	0.00064
C	0.00014
N	0.75086
O	0.23555
Ar	0.01281

4.2.2.2.3. Photons and Dose Calculations

As mentioned before the photon calculations were divided into the same two steps. First step was achieved without involving the phantom as well as the vehicle models. The incident photons calculations on the same size of a coupling cylinder surface were completed using SSW feature in MCNP. By using SSW feature, energy, position, and direction vector of the uncollided and scattered photons from semi-infinite cloud sources were recorded. The recorded incident photons in the SSW step were then used for the SSR step which including the phantom inside of a vehicle in order to be used for shielded dose calculations. In this step, the inside of the coupling cylinder volume was filled with air.

The next step for photon calculations was to determine the dose rate coefficients in male and female mathematical phantom using the recorded photons from the first step. This recorded incident photons were employed as source definition using the SSR feature. In this step, each phantom was located inside of each vehicle model separately. The volume between the phantom and the coupling cylinder were filled with air, as well. For all photon transport calculations, tissue kerma approximation was assumed. The photon fluence was generated using average track-length estimator (F6:P tally) in MCNP. The tissue dose rate calculations were performed using photon fluence and tissue-specific kerma coefficients. Then the semi-infinite geometry was considered dividing the tissue dose by 2. Organ dose rate coefficients were computed for 17 discrete photon energies, three vehicle models, and two phantoms. Afterwards, calculation of the effective dose rate coefficient was performed using tissue weighting factors as recommended in ICRP Publication 103.

4.2.2.3. Trailer Contamination

A truck-trailer was modeled based on the actual size and dimensions of an average trailer as shown in Figure 7 and the dimensions can be found in Figure A-4. The same calculation SSW and SSR steps were applied for this scenario assuming uniformly distributed monoenergetic photon in a trailer with 1 Bq m^{-3} source strength; however, the coupling cylinder used here was changed to a larger one in order to enclose the trailer. The only difference in the calculation of trailer contamination than the methods explained prior was the energy range bounding the simulations. While recording the incident photons on

the coupling surface in the SSW step, the computation of organ dose rate coefficients could not be achieved for lower energies since the steel trailer acted as a shielding material and did not give results for lower energies. Thus, organ dose rate coefficients were computed for 11 discrete photon energies ranging from 0.15 to 3 MeV, three vehicle models, and two phantoms. Afterwards, calculation of the effective dose rate coefficient was performed using tissue weighting factors as recommended in ICRP Publication 103.

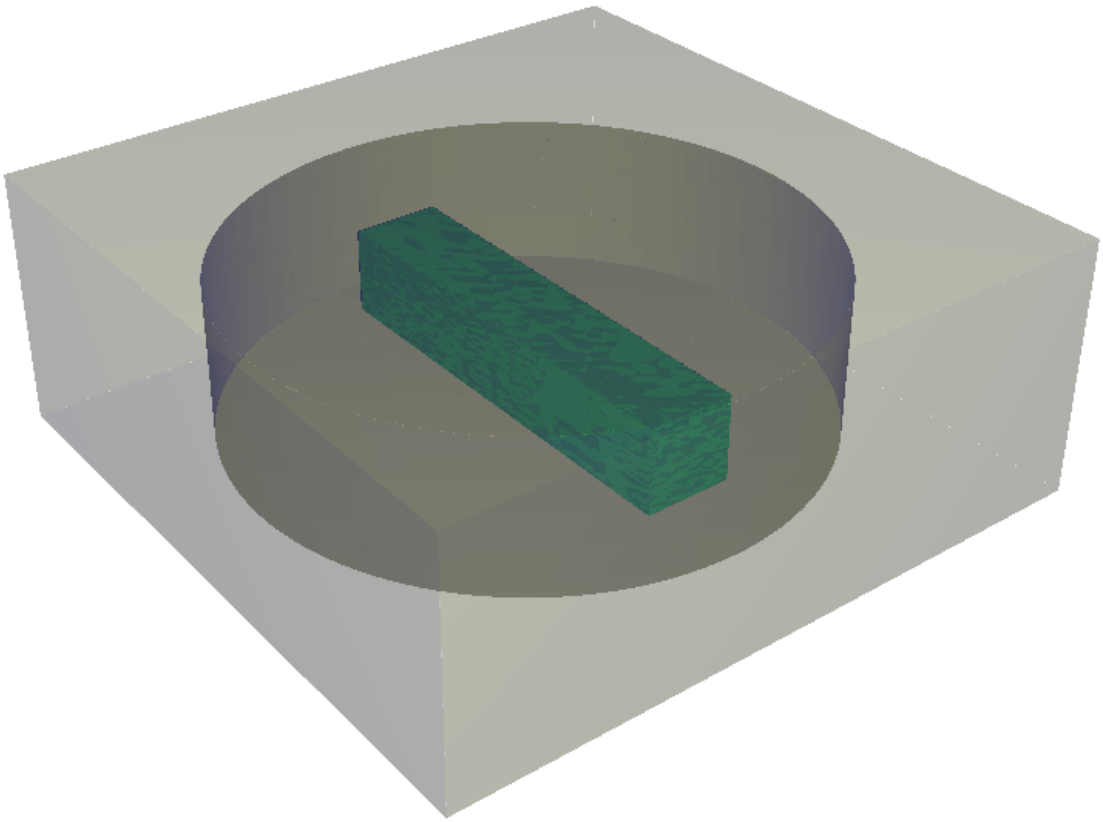

Figure 7. Truck-trailer used in SSW step for trailer contamination.

4.2.3. Unshielded Dose Calculations

As it is mentioned before, while the shielded dose was determined placing the vehicle and phantom inside of the coupling surface for each vehicle models in various contaminated environment, unshielded dose was taken when the vehicle was not present inside of the coupling surface using F6 tally. Unshielded dose used for RPF estimation was calculated applying the same two steps method. For the first step, the same SSW files used in the soil, air, and trailer contamination were employed. For the SSR step, each steel vehicle model was replaced with an air vehicle. The phantom was placed inside of the coupling cylinder without changing its position and location. Unshielded organ dose rate coefficients were computed for discrete photon energies depending on the vehicle model, three vehicle models, two phantoms, and three contaminated scenarios. Afterwards, calculation of the effective dose rate coefficient was performed using tissue weighting factors as recommended in ICRP Publication 103.

4.2.4. Variance Reduction

The complexity of the shielded geometry and the size of the contaminated environment necessitated the use of several variance reduction methods in different steps in order to minimize the uncertainty of the Monte Carlo simulations due to random error to sustain relative error lower than about 1%. Without variance reduction techniques for size of geometry and especially for lower energies, derivation of tissue dose rates would not be conducted in a computationally efficient manner within a reasonable timeframe to reach the desired statistical convergence [47]. For the same reason, low energy photon

sources for the dose rate calculations could not considered here. One of the main considerations was to employ sufficient particles and the 10 statistical checks reported by the MCNP6 code as convergence of the tallies. For the SSW step, exponential transform path-length stretching was used for all exposure scenarios. This method helped to achieve recording adequate number of particles. For the SSR step, since there were shielding material, weight-window generator and geometry splitting with Russian roulette were employed for the shielding material. The importance of the shielding material cells was increased by splitting the geometry with a few mean free path thicknesses depending on the source energy. The particle weights were altered by weight window generator. When the particles entered a cell and their weight was higher than the upper limit of the window, they were split into particle as having a weight within the window. These weight window data were reported in the MCNP output files and the problem was rerun altering the input file with the generated weight window data.

4.2.5. RPF Calculations

The protection factors for the transport of radioactive material were estimated using the ratio of unshielded dose over shielded dose employing Equation 1. The RPF values were computed for the combinations of various discrete photon energies depending on the vehicle design, three vehicle models, three contamination scenarios, and two mathematical phantoms. The RPF values for different types of vehicles in a different contaminated environment could be tabulated for radionuclides using a radionuclide interpolator which utilizes the ICRP Publication 107 Nuclear Decay Database [48]. The

photon energy and intensity data can be found in Table A-4. For interpolation, only photons without including bremsstrahlung were considered. The radionuclide-specific protection factors were determined employing unshielded radionuclide-specific dose rate data and shielded radionuclide-specific dose rate data. Generated radionuclides are shown in Table 9 and these radionuclides were chosen based on RAM sources mostly used in nuclear devices, nuclear medicine, and released from an event of cask accident [36], radiological dispersal device (RDD) (i.e., "dirty-bomb") event [49], fission products and actinides for contaminant exposure within the first 48 hours after a fission-based weapon detonation and longer-term exposure, and reactor accidents [50].

Table 9. Generated radionuclides for RPF values.

Nuclear Device/Medicine	**RDD**	**Fission products/ actinides**	**Reactor Accidents**	
^{22}Na	^{60}Co	^{91}Sr:^{91m}Y	^{95}Nb	^{137}Cs:^{137m}Ba
^{60}Co	^{131}I	^{95}Zr:^{95}Mo	^{95m}Nb	^{140}Ba
^{85}Kr	^{137}Cs	^{97}Zr:^{97}Nb	^{95}Zr	^{140}La
^{99m}Tc	^{192}Ir	^{99}Mo:^{99m}Tc	^{103}Ru	^{141}Ce
^{131}I	^{226}Ra	^{106}Ru:^{106}Rh	^{125}Sb	^{144}Ce
^{137}Cs	^{235}U	^{131m}Te: ^{131}I	^{127}Te	^{144}Pr
^{192}Ir	^{239}Pu	^{132}Te: ^{132}I	^{129}Te	^{147}Nd
^{241}Am	^{241}Am	^{137}Cs	^{129m}Te	^{148}Pm
^{252}Cf	^{252}Cf	^{144}Ce:^{144}Pr	^{131}I	^{148m}Pm
			^{134}Cs	^{154}Eu
			^{136}Cs	^{156}Eu

5. RESULTS

5.1. Incident-free Condition of Transport

As described in Section 3, the purpose of this incident-free transport analysis is to show the difference between the RADTRAN transport code which uses the simplified models and the Monte Carlo analysis using modeled package and a phantom. In order to make a detailed comparison, simplified point and line source models in RADTRAN, itself, were also simulated in MCNP and sex-averaged effective dose rate was determined using phantoms models.

Figure 8 summarizes the effective dose rate data as a function of various source-to-receptor distances, varying from 0.1 m to 10 m. This plot shows the results from RADTRAN incident-free analysis for handlers, sex-averaged dose rate data with respect to a modeled Type A package, and sex-averaged effective dose rate data with respect to simplified point and line source model simulated in MCNP. To be able to distinguish two different model, Figure 8 is divided into two separate plots at 2 m source-to-receptor distance. Figures 9 and 10 show plots of line and point source models separately. The important point to be considered when modeling the point-line source version of an actual package was that RADTRAN takes the distance between receptor-to-source from the geometrical center of the package instead of the package surface. Comparing the three

results, it can be seen that the plots show the distance between the phantom and the package surface.

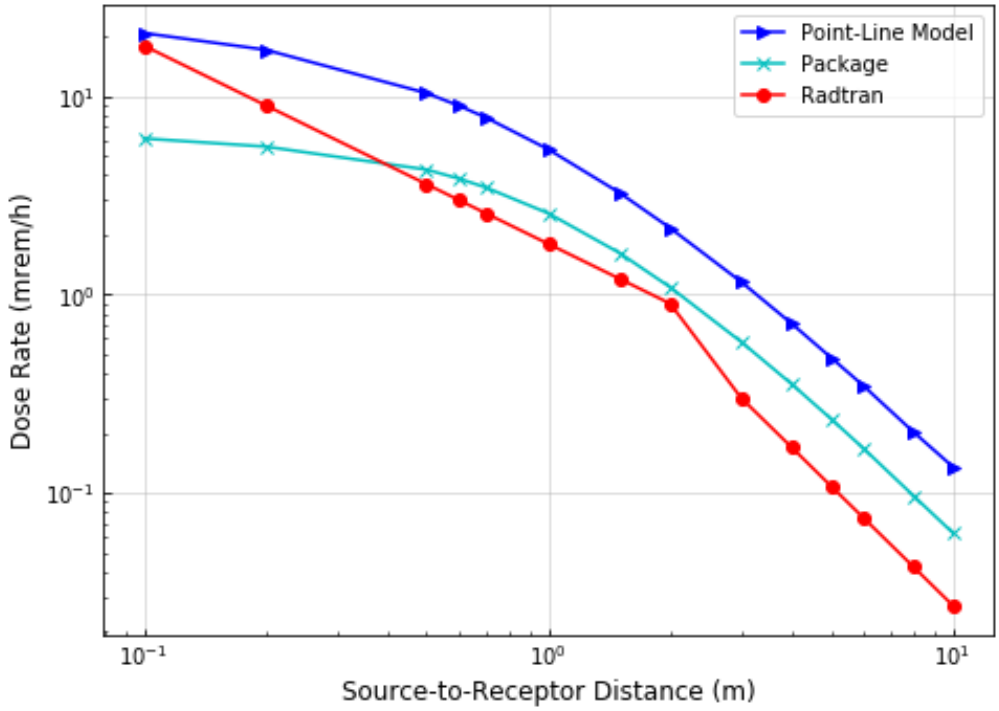

Figure 8. Dose rate as a function of source-to-receptor distance resulted from RADTRAN, effective dose rate resulted from modeled Type A package with phantom, and simplified point and line source models.

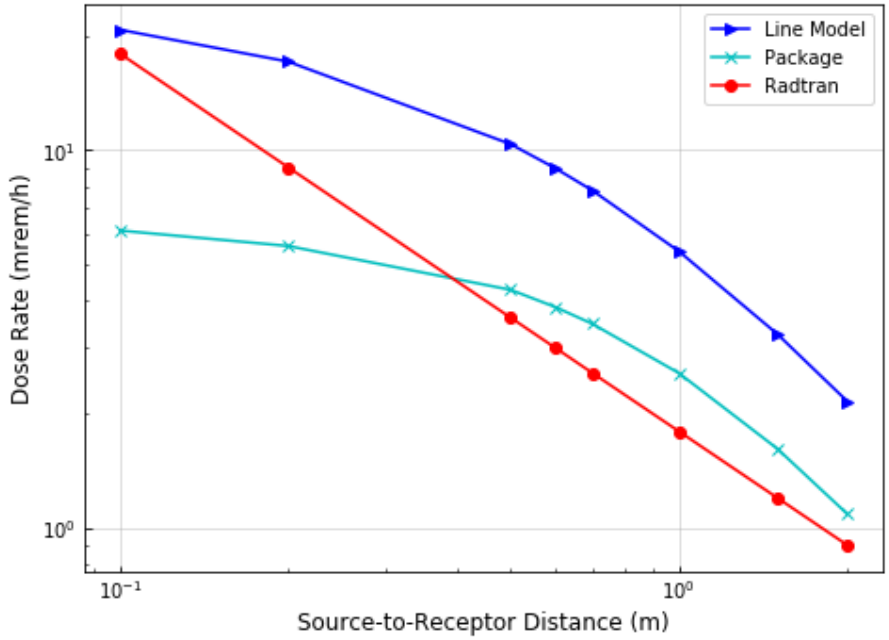

Figure 9. Dose rate as a function of source-to-receptor distance resulted from RADTRAN, effective dose rate resulted from modeled Type A package with phantom, and simplified line source model.

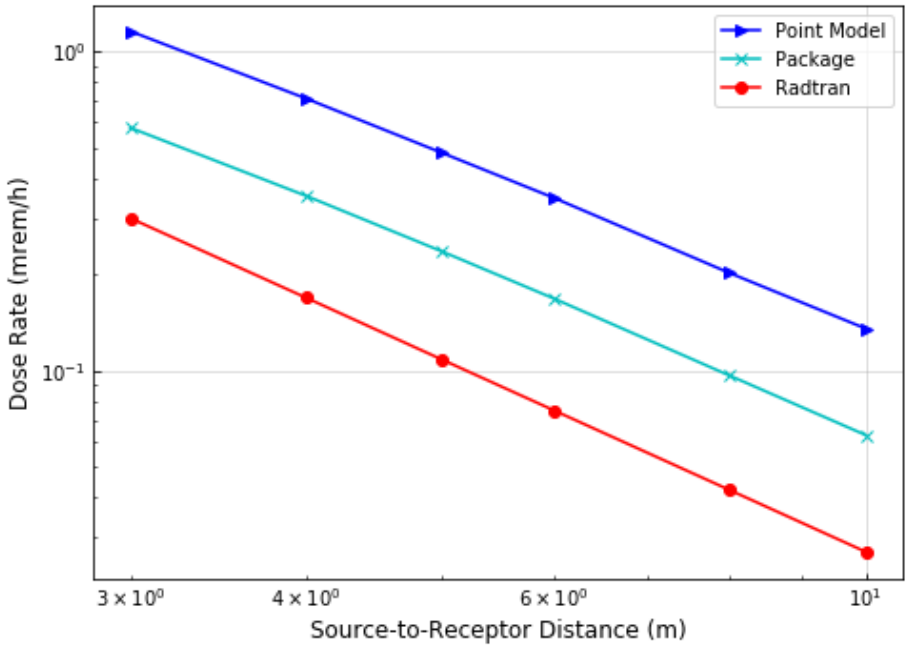

Figure 10. Dose rate as a function of source-to-receptor distance resulted from RADTRAN, effective dose rate resulted from modeled Type A package with phantom, and simplified point source model.

5.2. Hypothetical Incident Condition of Transport

5.2.1. Benchmarking

Benchmarking effort were conducted by comparing the effective dose rate data for unshielded analysis done for this work and the adopted works from FGR 15 [33] and ICRP 144 [38] for soil and air contamination scenarios. However, the computational geometries are similar, they are not the same regarding the phantom position and the size of the coupling cylinder used in the SSW step. Figure 11 shows the effective dose rate data as a function of photon energy resulted from the soil contamination scenario. Figure 12 displays the plot of the same results for air contamination scenario.

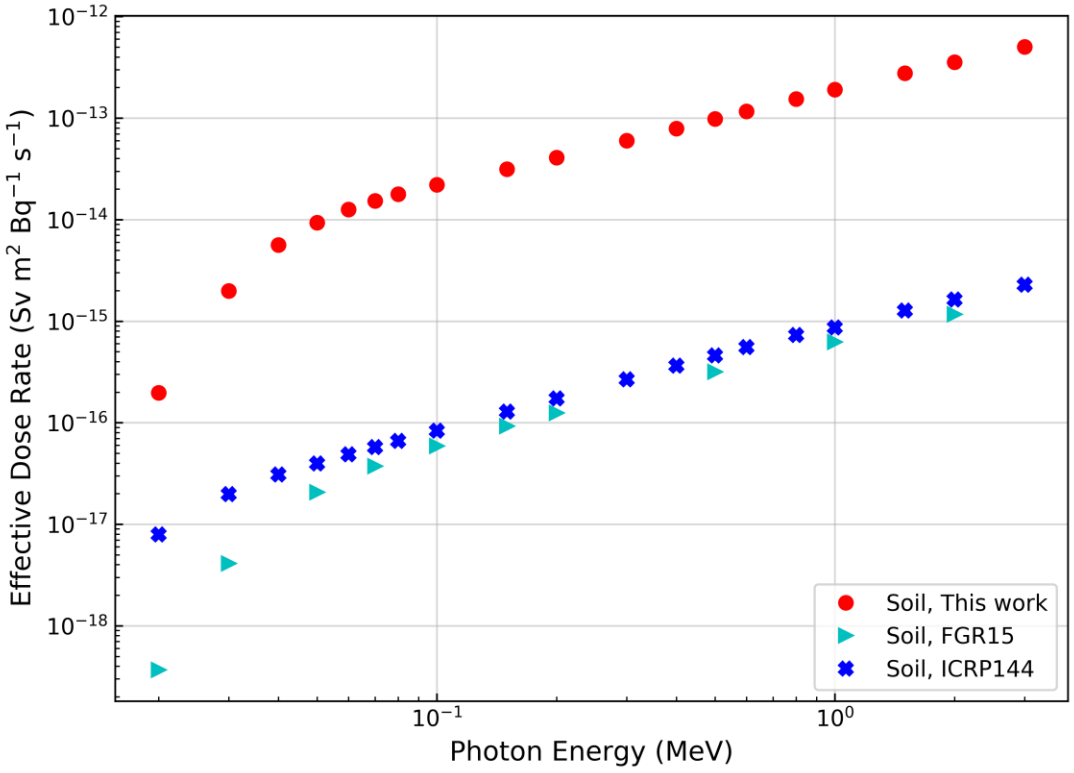

Figure 11. Sex-averaged effective dose rate coefficients for soil contamination. Also shown are the results of FGR 15 and ICRP 144.

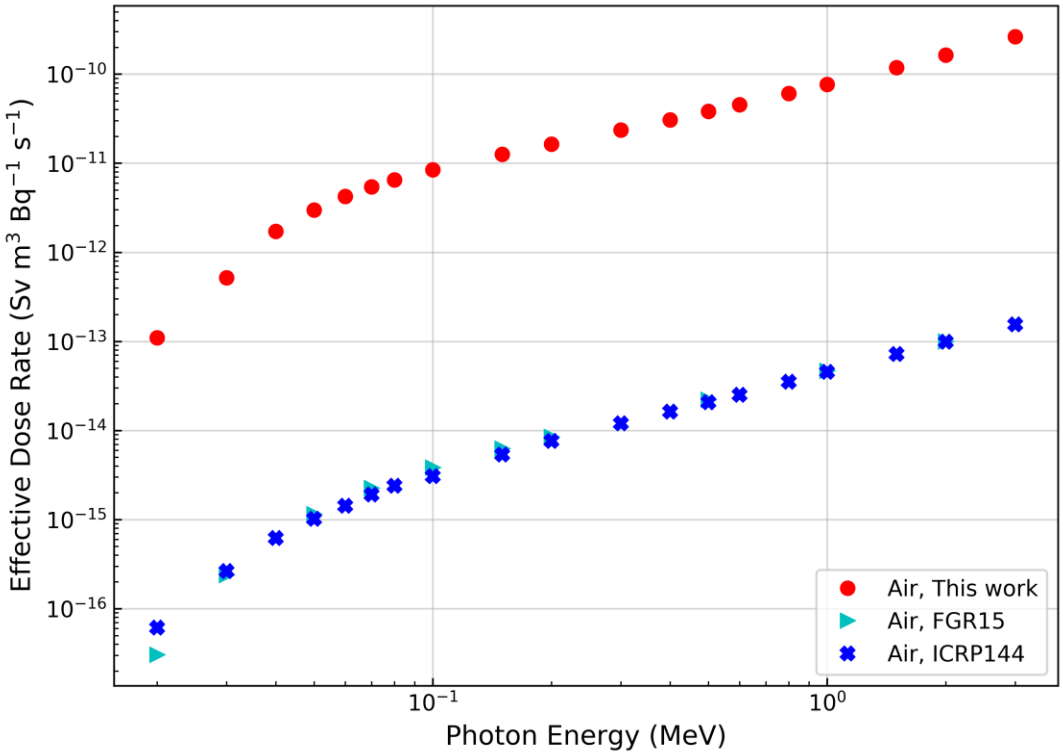

Figure 12. Sex-averaged effective dose rate coefficients for air contamination. Also shown are the results of FGR 15 and ICRP 144.

5.3. Shielded and Unshielded Effective Dose Rates

Figures 13-15 summarize the sex-averaged effective dose rate coefficients from shielded and unshielded simulations for soil, air, and trailer contamination scenarios, respectively. While unshielded dose rate data were taken when steel vehicle models were replaced with the air geometry in the SSR step, shielded simulations results are shown for 1-cm-thick box, 1-in-thick box, and more realistic vehicle model. For 1-cm-thick box, the results were taken for 0.04-3 MeV energy range; for 1-in-thick box, the results were taken for 0.06-3 MeV energy range; and for realistic vehicle model, the results were taken for 0.15-3 MeV energy range. Below these energy ranges, zero-tally were observed. These data were then used for energy dependent RPF values which is shown in the next section.

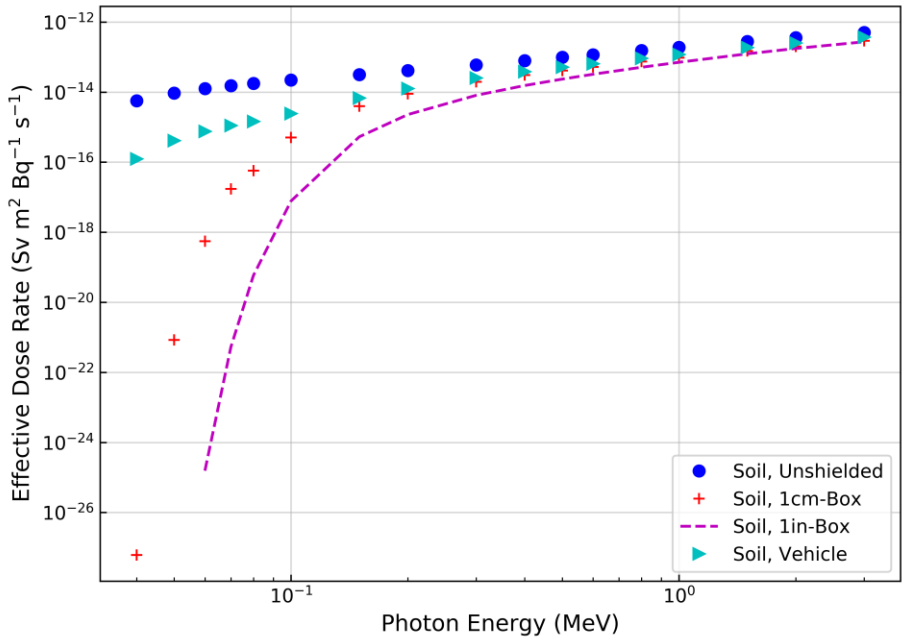

Figure 13. Sex-averaged effective dose rate coefficients for soil contamination for unshielded and shielded phantom. Shielded phantom results are shown for 1-cm-thick box, 1-in-thick box, and more realistic vehicle model.

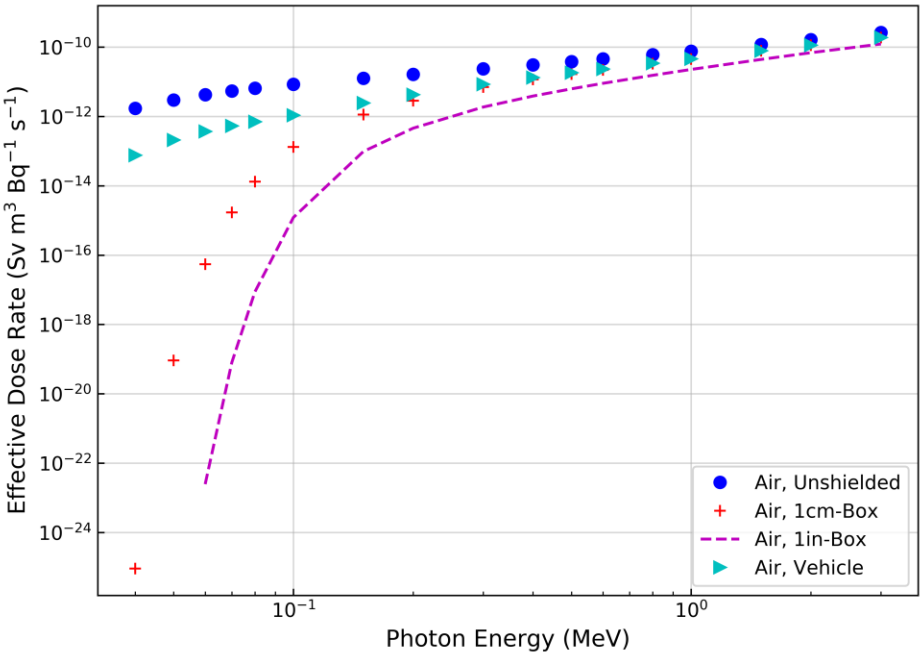

Figure 14. Sex-averaged effective dose rate coefficients for air contamination for unshielded and shielded phantom. Shielded phantom results are shown for 1-cm-thick box, 1-in-thick box, and more realistic vehicle model.

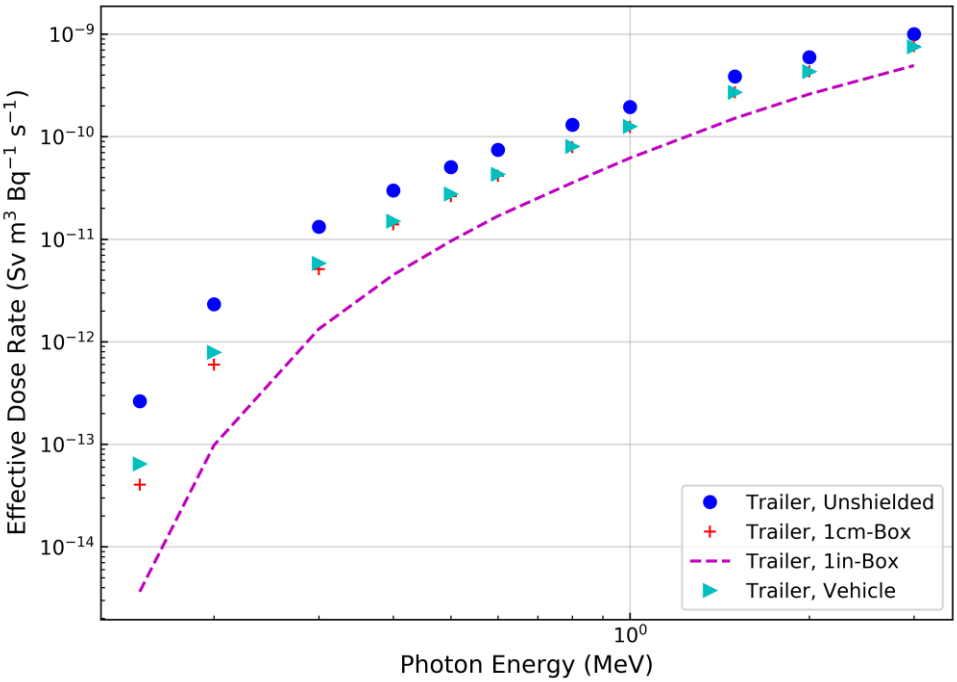

Figure 15. Sex-averaged effective dose rate coefficients for truck-trailer contamination for unshielded and shielded phantom. Shielded phantom results are shown for 1-cm-thick box, 1-in-thick box, and more realistic vehicle model.

5.3.1. Radiation Protection Factors

The second aim of this work was to determine gamma radiation protection factors of the different vehicle models for male and female mathematical phantoms on the driver seat, from external exposure to photons emitted by radionuclides distributed in air, soil, and inside of a truck-trailer.

Figures 16-18 display the plots of radiation protection factors for 1-cm-thick box, 1-in-thick box, and more realistic vehicle model resulted from the soil, air, and trailer contaminated environments, respectively. These RPFs were calculated by dividing the unshielded sex-averaged effective dose rate data to shielded sex-averaged effective dose rate data for 1-cm-thick box, 1-in-thick box, and more realistic vehicle model.

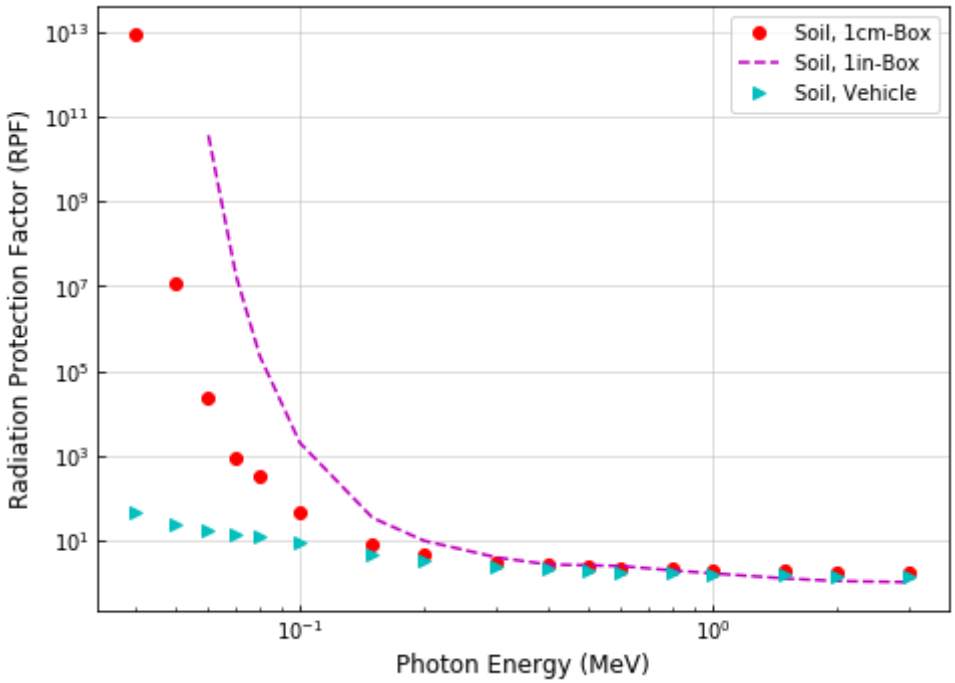

Figure 16. Calculated radiation protection factors for soil contamination for 1-cm-thick box, 1-in-thick box, and more realistic vehicle model.

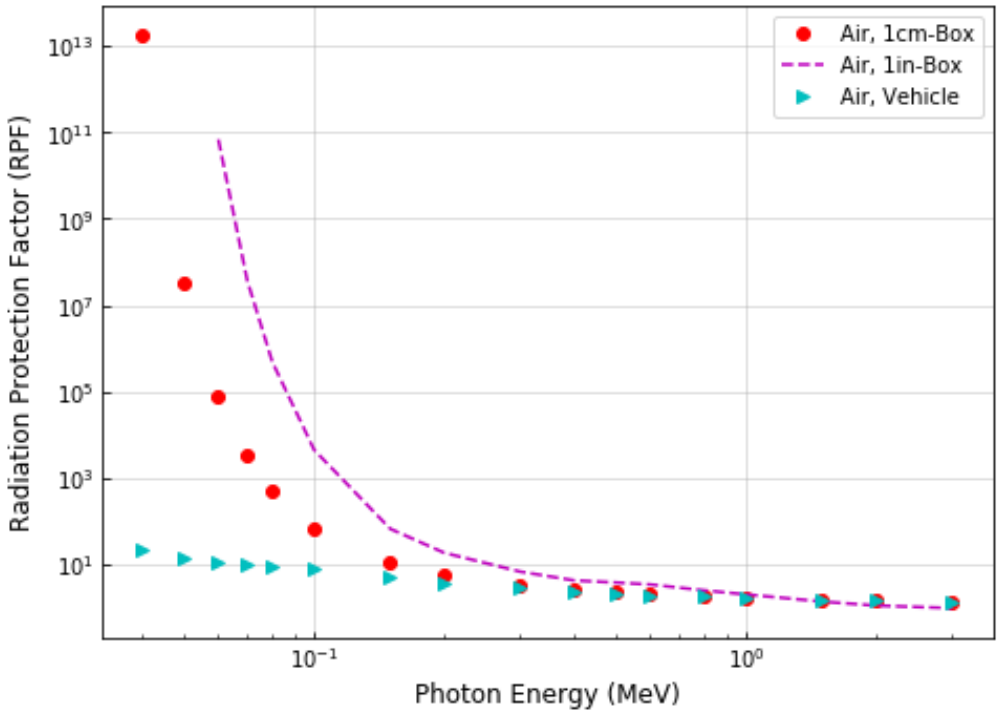

Figure 17. Calculated radiation protection factors for air contamination for 1-cm-thick box, 1-in-thick box, and more realistic vehicle model.

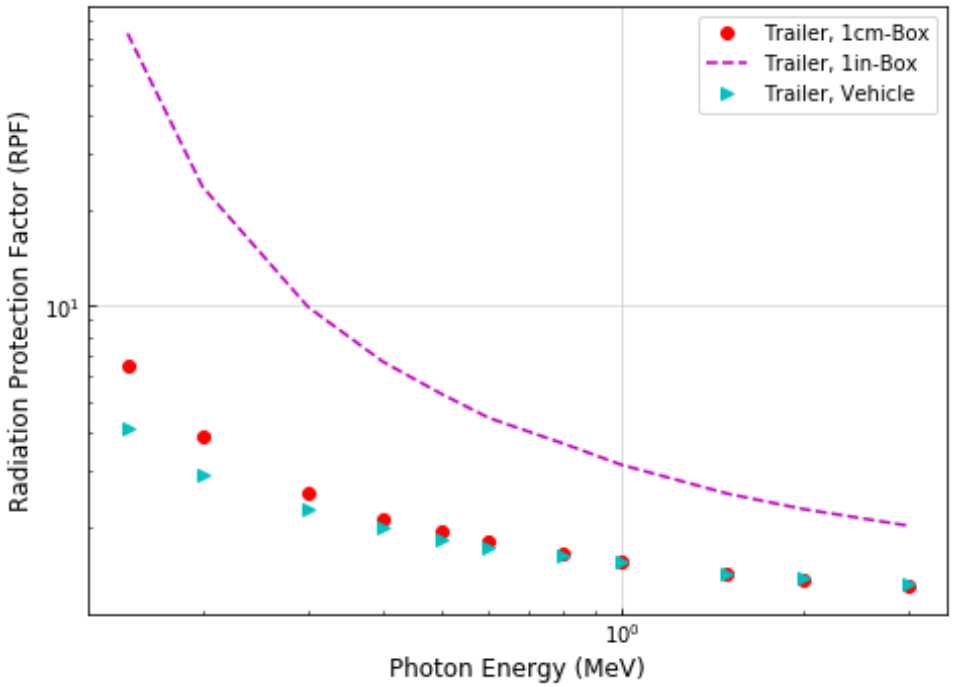

Figure 18. Calculated radiation protection factors for truck-trailer contamination for 1-cm-thick box, 1-in-thick box, and more realistic vehicle model.

Table 10 provides an overview of the energy values where the protection factor is equal to 2, meaning 50 percent of the photons will be protected by the vehicle, for each vehicle model in each contaminated environment scenario. Table 11 displays the percentages of the unprotected effective dose rate received from photons with 2 MeV energy.

Table 10. Energy values where the protection factor is equal to about 2.

	Soil Contamination	Air Contamination	Trailer contamination
1-cm-box	0.7 MeV	0.6 MeV	0.5 MeV
1-in-box	0.8 MeV	1.0 MeV	3.0 MeV
Vehicle	0.5 MeV	0.5 MeV	0.4 MeV

Table 11. Percentage of unprotected dose rate received from 2 MeV photons.

	Soil Contamination	Air Contamination	Trailer contamination
1-cm-box	56%	69%	73%
1-in-box	93%	90%	44%
Vehicle	70%	69%	72%

Table 12 represents the committed time period the emergency responder could spend in the soil contaminated environment until reaching to the reference radiation safety dose limit for each vehicle model. The reference value of lifesaving or protection of large populations for emergency responder radiation safety is provided by the National Council on Radiation Protection and Measurements (NCRP) Report 179 as 250 mSv [22]. Saito et al. [51] provided the maximum deposition density data for radionuclides from the Fukushima Dai-ichi Nuclear Power Plant (NPP) accident by collecting large-scale soil samples which are about 10,915 at 2168 locations. These radionuclides were chosen based on the dominant gamma-ray emitting radionuclides deposited on the ground. ^{134}Cs and ^{137}Cs were detected at every soil sampling location [51].

Table 12. Calculated stay time to reach NCRP dose limits in a vehicle, 1-cm-box, and 1-in-box from Fukushima contamination scenario for the reference maximum deposition density.

	Maximum deposition density (Bq/m^2)	Time for vehicle (h)	Time for 1-cm-box (h)	Time for 1-in-box (h)
^{134}Cs	1.4×10^7	1.65×10^1	3.53×10^1	5.36×10^1
^{137}Cs	1.5×10^7	2.67×10^1	8.74×10^1	1.36×10^2
^{131}I	5.5×10^4	3.53×10^4	4.44×10^4	8.81×10^4
^{129m}Te	2.7×10^6	7.78×10^3	9.66×10^3	1.47×10^4

5.3.1.1. Radionuclide-specific Protection Factors

Table 13 shows the generated RPF values of radionuclides for 1-cm box, 1-in box, and modeled vehicle in soil, air, and trailer contaminated environment using a radionuclide interpolator which utilizes the ICRP Publication 107 Nuclear Decay Database [48].

Table 13. Radionuclide-specific RPFs.

Nuclide	Soil Contamination			Air Contamination			Trailer Contamination		
	1-cm box	1-in box	vehicle	1-cm box	1-in box	vehicle	1-cm box	1-in box	vehicle
^{241}Am	3416.52	11189.36	18.20	3456.39	13412.07	12.18	5.72	36.81	5.72
^{137}Cs:^{137m}Ba	2.18	3.40	1.76	1.98	4.63	1.89	1.74	4.13	1.70
^{140}Ba	2.53	4.59	2.02	2.45	6.66	2.22	1.92	5.12	1.82
^{141}Ce	9.07	72.61	5.08	12.56	155.04	5.49	6.53	72.47	4.10
^{144}Ce:^{144}Pr	13.40	130.51	6.39	18.46	272.9	6.40	6.57	73.30	4.12
^{252}Cf	1.98	2.50	1.58	1.65	2.93	1.62	1.42	2.42	1.42
^{60}Co	1.90	2.41	1.53	1.59	2.95	1.57	1.48	2.76	1.47
^{134}Cs	2.14	3.25	1.73	1.92	4.35	1.84	1.70	3.85	1.47
^{136}Cs	2.09	2.95	1.69	1.82	3.76	1.76	1.58	3.25	1.57
^{154}Eu	2.09	2.85	1.68	1.79	3.56	1.73	1.54	3.03	1.53
^{156}Eu	1.92	2.40	1.54	1.59	2.87	1.57	1.45	2.60	1.45
^{131}I: ^{131m}Te	2.65	5.27	2.11	2.70	8.13	2.38	2.08	6.08	1.95
^{132}I: ^{132}Te	2.09	3.04	1.69	1.84	3.95	1.78	1.62	3.44	1.60
^{192}Ir	2.71	5.46	2.15	2.78	8.46	2.43	2.09	6.08	1.95
^{85}Kr	2.35	4.09	1.90	2.25	5.95	2.08	1.91	5.14	1.82
^{140}La	1.94	2.46	1.55	1.62	2.97	1.59	1.45	2.63	1.45

Table 13. Radionuclide-specific RPFs. (continued)

Nuclide	Soil Contamination			Air Contamination			Trailer Contamination		
	1-cm box	1-in box	vehicle	1-cm box	1-in box	vehicle	1-cm box	1-in box	vehicle
^{22}Na	1.90	2.39	1.53	1.58	2.93	1.57	1.47	2.75	1.47
^{95}Nb	2.10	3.09	1.70	1.85	4.09	1.79	1.67	3.77	1.64
^{95m}Nb	3.96	13.00	2.93	4.65	23.42	3.44	3.08	13.68	2.55
^{147}Nd	3.41	6.27	2.61	3.21	8.81	2.74	1.91	5.05	1.82
^{148}Pm	1.98	2.61	1.59	1.68	3.24	1.65	1.50	2.86	1.49
^{148m}Pm	2.22	3.50	1.79	2.03	4.78	1.92	1.74	4.04	1.69
^{144}Pr	1.89	2.34	1.52	1.56	2.77	1.55	1.43	2.48	1.43
^{239}Pu	30.83	157.84	16.10	26.21	166.41	11.77	2.29	7.30	2.10
^{226}Ra	5.61	24.89	3.73	7.14	50.11	4.31	4.06	25.09	3.03
^{106}Ru:^{106}Rh	2.23	3.54	1.80	2.05	4.84	1.94	1.73	3.97	1.68
^{103}Ru	2.37	4.16	1.91	2.28	6.07	2.10	1.92	5.20	1.83
^{125}Sb	2.44	4.28	1.96	2.33	6.11	2.14	1.87	4.83	1.79
^{91}Sr:^{91m}Y	2.04	2.85	1.65	1.76	3.65	1.72	1.59	3.29	1.58
^{99m}Tc:^{99}Mo	9.43	78.56	5.09	13.31	170.81	5.52	6.53	72.56	4.10
^{127}Te	2.63	5.20	2.10	2.67	8.03	2.36	2.11	6.48	1.97
^{129}Te	2.49	4.41	2.00	2.35	6.12	2.16	1.82	4.45	1.75
^{129m}Te	2.47	4.09	1.99	2.15	5.19	2.04	1.71	3.94	1.67
^{235}U	5.88	26.81	3.84	7.52	53.59	4.41	3.96	23.32	2.99
^{95}Zr:^{95}Mo	2.11	3.15	1.71	1.88	4.19	1.87	1.69	3.84	1.65
^{97}Zr:^{97}Nb	2.10	3.08	1.70	1.85	4.04	1.79	1.65	3.59	1.62

6. DISCUSSIONS

6.1. RADTRAN Analysis

The first objective of this work was to compare the simplified models used in RADTRAN code and validate these models with the computational efforts by modeling the actual package and the simplified models in MCNP. The comparison was performed simulating the same representative Type A package described in previous work [27]. The external radiation field of 1.2 mrem/h at 1 m distance from the package surface, the TI value, consisted of 100% gamma radiation was assumed. Regulations in 10 CFR Part 71 specify that the external dose rate at two meters from the package surface should not exceed 10 mrem/h (0.1 mSv/h). This is equivalent to about 14 mrem/h at one meter from the package surface for a "critical dimension" of about 5 meters [1]. All simulations and the RADTRAN results were consisted with this statement. It must be noted that both cases showed the expected 1/r and $1/r^2$ relationship between dose and the distance from the source due to the line and point source, respectively. Another finding was the effective dose rate coefficients from MCNP simulations were higher than the dose rates calculated in RADTRAN. These differences can be explained in part by the absorption and reflection from the ground and the actual package surface are neglected by the RADTRAN code. Another explanation can be any energy distribution effects are not considered in RADTRAN by assuming the gamma attenuation and the buildup as to be 1 for all energies. However, computational method and the adopted line and point source model in the code was quite similar, the code was found conservative for the line source model when the distance between package and the receptor is short. It can be stated that the instead of

using computational sources and time, code is proved to work well especially when source-to-receptor distance is bigger than the critical package dimension.

6.2. RPF

This study set out with the aim of assessing the RPF values of vehicles for civilian and military purposes. For that reason, different vehicle models and contaminated scenarios were simulated. The main idea was to blend two separate works together in order to have a solution for the public concern and emergency responders. One work was done previously on determination of RPF for simple steel box but this work was limited for the simple steel box and fallout gamma radiation and cannot be extended the scenario when the vehicle is surrounded by contaminated environment [6]. The other works were done for the evaluation of the contaminated environment but they are not included any shielding material [33, 34, 46]. The current research was performed combining these two approaches altering the geometries and employing simple and more realistic vehicle models to prove that this approach can be implemented for the advanced and different types of vehicle considering the different position of phantoms.

For benchmark effort, effective dose rate data for unshielded analysis done for this work were compared to the adopted work FGR 15 [33]and ICRP 144 [38] for soil and air contamination scenarios as shown in Figures 11 and 12. However, while the computational geometries are similar, they are not the same regarding the phantom position and the size of the coupling cylinder used in SSW step. The observed increase in the benchmark could be caused by the phantom position and the computational geometry since for the sitting

positioned phantom, the upper body would not be protected by the attenuation from the lower body and the coupling cylinder was chosen bigger than the comparison works to be able to fit the vehicle models. Thus, unshielded contaminated scenario in this work was resulted in a reasonable higher dose rate. This variation in the effective dose rate is consistent with studies considering the effect of postures in idealized radiation fields by Dewji et al.[12] and Bales et al. [13]

The sex-averaged effective dose rate coefficients as a function of incident photon energy for soil, air, and trailer contamination scenarios, the same trend is observed. Regarding the shielded simulations, it was expected that the dose rate in the modeled vehicle would be higher than the one in 1-cm-box. A possible explanation for this might be that incident photon particles can be easily attenuated in the fiberglass material. The lowest dose rate data were taken from inside of the 1-in-box regarding increased thickness of the steel shielding material. The observed difference between unshielded and shielded effective dose rate for phantom are likely to be related to the photon attenuation of dominant components of the vehicle material (^{56}Fe) and the air material (^{14}N).

Turning now to the radiation protection factors for vehicles as a function of photon energy, when comparing the soil, air, and trailer RPFs, they should be evaluated separately because of the different radiation levels in a contaminated environment. The effective dose rate for the unshielded contaminated soil environment is ranged from the order of 10^{-14} to 10^{-12} Sv m^2 Bq^{-1} s^{-1}, air environment is ranged from almost 10^{-12} to 10^{-10} Sv m^3 Bq^{-1} s^{-1}, and finally the trailer contaminated environment shows this range from 10^{-12} to 10^{-9} Sv m^3 Bq^{-1} s^{-1}. It must be underlined that for 1-cm-thick box, the results were taken for 0.04-3 MeV

energy range; for 1-in-thick box, the results were taken for 0.06-3 MeV energy range; and for realistic vehicle model, the results were taken for 0.15-3 MeV energy range. Below these energy ranges, zero-tally were observed. In all the simulations, the relative error was always under 1% applying the several variance reduction techniques.

The most noteworthy aspect of the RPF data is at the higher energies. As mentioned prior, the lowest dose rate data were taken from the 1-in-box; however, shielding effectiveness started at lower protection levels of 1-cm-box and vehicle model. One explanation is that the photon energy deposition from increased Compton interactions will be higher in steel with the increasing photon energy and the amount of shielding material. While this aspect can be observed above 1.5 MeV for soil contamination, above 2 MeV for air contamination, this difference has not been found in trailer contamination scenario. It is likely due to the scope of energy range of this work was not enough to observe this trend for trailer contamination.

The vehicle models offer protection from photons with lower energies and thus, relatively higher RPFs. As given in Table 10, the phantom is well-shielded until those energies with relatively high RPF values and after that, the protection level falls below the 50 percent. However, 1-in-box has the highest protection behavior until those energies shown in the Table 10, the breakdown of 1-in-box can be observed from Table 11 that its protection level is less than 1-cm-box and vehicle for soil and air contaminated environments. Since this difference has not been found elsewhere but it seems possible that these results may be due to increased scattering interactions of higher energy photons with the 1-in-box.

Prior studies that have noted the protection factor for 1-in-thick simple steel box is about 1.4 for photon energies 2.0 MeV and higher. Hence, for all photon energies, the shielded dose data would not be higher than about 70% the unprotected dose, which will be received by tissue from the same well-defined radiation field [6]. It can be seen from the Table 11 that the 93 percent of the dose will not be protected by the 1-in-box for soil contaminated environment, 90 percent for air contaminated environment, and 44 percent for trailer contaminated environment. The reason of the protection of the vehicles are relatively better in trailer contaminated environment can be correlated to the fact that the photons are already protected by the trailer before contaminating the environment.

Compared to the previous study by Takahara et al. [30], the dose reduction factor of vehicle models for air submersion (cloudshine), which then converted into RPF, is summarized in Table 3. In this work by Takahara, the RPF values for modeled vehicle was found to be 2.34, 1.66, and 1.51 for 0.4 MeV, 1 MeV, and 1.5 MeV photon energies, respectively. For the soil surface contamination (groundshine) scenario, data shown in the Table 4 were evaluated considering only the contribution of ^{137}Cs. The RPF value for ^{137}Cs source was found to be 1.76 for the current work for the relaxation mass depth of 0.5 g cm^{-2} which is equal to 3 mm for a soil density of 1.6 x 10^3 kg m^{-3}. However, the RPF values for this work were slightly higher than the previous work by Takahara. The differences in both cloudshine and groundshine may derive from the greater thickness and the amount of window used for the modeled vehicle. The current study is also compared to the experimental data provided by Takahara et al. [30] for the modeled vehicle in a contaminated environment from the ^{137}Cs source dispersion in soil. While experimental

data ranges from 0.54 to 0.65, resulting in RPF values from 1.54 to 1.85, the RPF value for ^{137}Cs source was found to be 1.76 for this work as mentioned before. It can be concluded that a reasonable agreement was achieved between the modeled vehicle in this study and the experimental measurement in case of a nuclear accident.

Based on the soil contamination dose data of all 3 types of vehicles, reference value of lifesaving or protection of large populations for emergency responder radiation safety provided by the National Council on Radiation Protection and Measurements (NCRP) Report 17 , which is 250 mSv, would be reached in a committed time period given in Table 12. Even every minute will be valuable for the emergency responders in the case of a nuclear incident resulted in radiological dispersion, considering the differences in the Table 12 for time data between the modeled vehicle and the box. Thus, the vehicle data will better inform the emergency responders about how much time they could spend in contaminated environments since the RPF values were overestimated for the box models.

7. CONCLUSION

Using simplified models plays a vital role for radiation protection world to reduce computational time without using full-scale resources, but also needs to be validated with developed computational efforts representative of the latest models and recommendations. Although many efforts have been undertaken to calculate the radiation protection factor for vehicles, it is observed that they are limited due to evaluating prompt radiation fields from nuclear weapons. Therefore, there is necessary to advance estimation of radiation protection factor for realistic vehicle model in a contaminated environment, such as cloudshine and groundshine during Fukushima-like events, for both military and civilian purposes. The initial effort for incident-free analysis employing simplified models used in the transport code is proven to adequately estimate the dose received by handler. The second aim of this study was to investigate RPFs of different vehicle models in a several contaminated environments. The present study was designed to characterize the differences between various models used in transport risk analyses code itself as well as better informing the first responders and the general public about radiation protection for radioactive material transportation and consequence management.

Based on the benchmarking and comparisons between the previous studies and the current analysis, it can be concluded that as the effect of phantom posture and the use of complex structure for vehicle models surrounded by radiological contamination dispersed in the air and on the soil will better inform the emergency responders about emergency preparedness and consequence management in case of a transportation accidents or radiological dispersion. Although the study is based on photon interactions and do not

explain the impact of bremsstrahlung from beta-emitters, the findings suggests that future studies, which take these variables into account, on the current topic are therefore recommended to develop a detailed examination of RPF from transportation or RAM. Overall, RPF values were overestimated for the simple box models in general and the overestimation increases with the increasing thickness of the box models. Considering the experimental measurement taken from Fukushima prefecture with the RPFs ranged from 1.54 to 1.85 for vehicle models with various thicknesses, it can be also concluded that the simple box model overestimates the RPF, 2.18 for 1-cm-box and 3.4 for 1-in-box, for soil contamination resulted from the contribution of ^{137}Cs source, while the RPF of vehicle is 1.76 which is in the range of experimental result. The vehicle model protects 50% of the incident photons with 0.5 MeV energy and this percentage falls below 30% after 2 MeV photons. The calculated stay time in vehicle is found to be 16.5 hours for ^{134}Cs, 26.7 hours for ^{137}Cs, 3.53×10^{4} hours for ^{131}I, and 7.78×10^{3} hours for ^{129m}Te employing the maximum deposition density in soil after Fukushima Dai-ichi NPP accident. After these suggested committed time values, the emergency responders will reach the 250 mSv dose limit of lifesaving or protection of large population in the case of a nuclear accident. This work demonstrates a methodology for calculating and evaluating RPF values from transportation vehicle, and can be expanded for every gamma-emitting radionuclide and every type of vehicle through CAD implemented into MCNP surface input deck easily and which will be a substantial solution for emergency responders in both civilian and military purposes.

REFERENCES

1. Neuhauser, K., F. Kanipe, and R. Weiner, *RADTRAN 5 technical manual.* Albuquerque, NM: Sandia National Laboratories, 2000.
2. Yuan, Y., et al., *RISKIND: A computer program for calculating radiological consequences and health risks from transportation of spent nuclear fuel*. 1995, Argonne National Lab.
3. Arcieri, W., *RADTRAD: a simplified model for radionuclide transport and removal and dose estimation*. 2002, NUREG/CR-6604, Supplement 2, US Nuclear Regulatory Commission, Washington, DC.
4. Nuclear Regulatory Commission, *Final environmental statement on the transportation of radioactive material by air and other modes*. 1977, Nuclear Regulatory Commission.
5. Decker, A.W., *Verification and Validation Report for the Radiation Protection Factor Methodology using Monte-Carlo n-Particle Code, version 6*. 2018, Nuclear Science and Engineering Research Center West Point United States.
6. McHale, S. and A. Decker, *Estimating radiation protection factor (RPF) values for a simple surrogate vehicle using the MCNP6. 1 code.* Applied Radiation and Isotopes, 2019. **153**: p. 108825.
7. McHale, S.R., A.W. Decker, and B.K. Huff, *APPLICATION OF THE MCNP6. 1 CODE TO ESTIMATE THE DIRECTIONAL DEPENDENCE OF RADIATION PROTECTION FACTOR VALUES FOR A SIMPLE SURROGATE VEHICLE.* Radiation Protection Dosimetry, 2020.
8. International Commission on Radiological Units And Measuremets, *ICRU Report*. 1985.
9. International Commission on Radiological Protection, *ICRP publication 103.* Ann ICRP, 2007. **37**(2.4): p. 2.
10. Petoussi-Henss, N., et al., *ICRP Publication 116—the first ICRP/ICRU application of the male and female adult reference computational phantoms.* Physics in Medicine & Biology, 2014. **59**(18): p. 5209.
11. Eckerman, K., M. Cristy, and J. Ryman, *The ORNL mathematical phantom series. Oak Ridge, TN: Oak Ridge National Laboratory; 1996*. 2006.
12. Dewji, S., K.L. Reed, and M. Hiller, *Comparison of photon organ and effective dose coefficients for PIMAL stylized phantom in bent positions in standard irradiation geometries.* Radiation and Environmental Biophysics, 2017. **56**(3): p. 277-291.
13. Bales, K. and S. Dewji, *Comparison of Organ and Effective Photon Dose Coefficients for Reference Phantoms in Articulated and Upright Postures in Cranial and Caudal Irradiation Geometries.* Health Physics, 2019. **116**(5): p. 599-606.
14. Akkurt, H., et al., *PIMAL: computational phantom with moving arms and legs.* TRANSACTIONS-AMERICAN NUCLEAR SOCIETY, 2007. **96**: p. 396.

15. Akkurt, H. and K.F. Eckerman, *Development of PIMAL: mathematical phantom with moving arms and legs*. 2007, Oak Ridge National Lab.(ORNL), Oak Ridge, TN (United States).
16. Werner, C., *MCNP Users Manual-Code Version 6.2 Los Alamos National Laboratory Report LA-UR-17-29981*. 2017, Tech. rep.
17. Dewji, S. and M. Hiller, *PIMAL: phantom with moving arms and legs, version 4.1. 0. Rockville, MD: US Nuclear Regulatory Commission*. 2016, NUREG/CR-7243.
18. Bellamy, M.B., et al., *Comparison of monoenergetic photon organ dose rate coefficients for stylized and voxel phantoms submerged in air.* Radiation protection dosimetry, 2016. **172**(4): p. 367-374.
19. Hiller, M. and S.A. Dewji, *Comparison of monoenergetic photon organ dose rate coefficients for the female stylized and voxel phantoms submerged in air.* Radiation protection dosimetry, 2017. **175**(3): p. 336-343.
20. Griffin, K.T., et al., *Stylized versus voxel phantoms: a juxtaposition of organ depth distributions.* Physics in Medicine & Biology, 2020. **65**(6): p. 065007.
21. NRC, U., *NRC regulations, title 10 Code of federal regulations (10 CFR).* US Nuclear Regulatory Commission (US NRC), Rockville, MD, 2016.
22. Perle, S., *NCRP Report No. 179, Guidance for Emergency Response Dosimetry*. 2018, LWW.
23. Taylor, J. and S.L. Daniel, *RADTRAN II: Revised Computer Code to Analyze Transportation of Radioactive Material*. 1982, Sandia National Labs.
24. Madsen, M.M., et al., *RADTRAN III*. 1986, Sandia National Labs., Albuquerque, NM (USA); Science Applications ….
25. Neuhauser, K. and F. Kanipe, *RADTRAN 4.* Volume III, User Guide, SAND89-2370, Sandia National Laboratories, Albuquerque, New Mexico, 1992.
26. Weiner, R.F., et al., *RADTRAN 6 Technical Manual.* Sandia National Laboratories, SAND2014-0780, USA, 2014.
27. Steinman, R., R. Weiner, and K. Kearfott, *A comparison of transient dose model predictions and experimental measurements.* Health physics, 2002. **83**(4): p. 504-511.
28. Weiner, R. and K. Neuhauser, *Near-field radiation doses from transported spent nuclear fuel*. 1991, Sandia National Labs.
29. Burson, Z., *Environmental and fallout gamma radiation protection factors provided by civilian vehicles.* Health physics, 1974. **26**(1): p. 41-44.
30. Takahara, S., et al., *Dose-reduction effects of vehicles against gamma radiation in the case of a nuclear accident.* Health physics, 2018. **114**(1): p. 64-72.
31. International Commission on Radiological Protection, *ICRP Publication 74: Conversion coefficients for use in radiological protection against external radiation*. Vol. 23. 1996: Elsevier Health Sciences.
32. Bellamy, M., et al., *Effective dose rate coefficients for immersions in radioactive air and water.* Radiation protection dosimetry, 2017. **174**(2): p. 275-286.
33. Bellamy, M., et al., *EXTERNAL EXPOURE TO RADIONUCLIDES IN AIR, WATER AND SOIL*. 2019, EPA 402-R19-002. Federal Guidance Report.

34. Eckerman, K.F. and J.C. Ryman, *External exposure to radionuclides in air, water, and soil*. 1996, Oak Ridge National Lab.
35. Fritsch, F.N. and R.E. Carlson, *Monotone piecewise cubic interpolation.* SIAM Journal on Numerical Analysis, 1980. **17**(2): p. 238-246.
36. Chen, S. and A. Kapoor, *The Resource Handbook on DOE Transportation Risk Assessment*. 2003, Argonne National Laboratory, IL (US); USDOE Albuquerque Operations Office ….
37. Edling, D., *DOE(Department of Energy) Evaluation Document for DOT(Department of Transportation) 7 A Type A Packaging.* 1987.
38. Petoussi-Henss, N., et al., *ICRP Publication 144: Dose Coefficients for External Exposures to Environmental Sources.* Annals of the ICRP, 2020. **49**(2): p. 11-145.
39. McNeel, R., *Rhinoceros 5 User's Guide for Windows.* 2016.
40. Kos, B. and L. Snoj, *On using Grasshopper add-on for CAD to MCNP conversion.* PHYSOR, Sun Valley, USA, 2016.
41. Saito, K., et al., *Calculation of organ doses from environmental gamma rays using human phantoms and Monte Carlo methods Part I: Monoenergetic Sources and Natural Radionuclides in the Ground Technical Report GSF–2/90 IAEA.* Neuherberg: GSF-National Research Center for Environment and Health, 1990.
42. International Commission on Radiological Units And Measurements, *ICRU Publication 53*. 1994: Bethesda.
43. Dillman, L.T., *Absorbed gamma dose rate for immersion in a semi-infinite radioactive cloud.* Health Physics, 1974. **27**(6): p. 571-580.
44. Poston, J. and W. Snyder, *A model for exposure to a semi-infinite cloud of a photon emitter.* Health physics, 1974. **26**(4): p. 287-293.
45. Kocher, D.C., *Dose-rate conversion factors for external exposure to photons and electrons*. 1981, Oak Ridge National Lab., TN (USA).
46. Eckerman, K.F. and J.C. Ryman, *External exposure to radionuclides in air, water, and soil, Federal Guidance Report 12.* ORNL, 1993.
47. Fitzgerald, J.J., G.L. Brownell, and F.J. Mahoney, *Mathematical theory of radiation dosimetry*. 1967: Gordon and Breach.
48. Eckerman, K. and A. Endo, *ICRP Publication 107. Nuclear decay data for dosimetric calculations.* Annals of the ICRP, 2008. **38**(3): p. 7.
49. Rump, A., et al., *Medical management of victims contaminated with radionuclides after a "dirty bomb" attack.* Military medical research, 2018. **5**(1): p. 1-10.
50. Dewji, S., et al., *Estimation of External Contamination and Exposure Rates Due to Fission Product Release.* Health physics, 2020. **119**(2): p. 163-175.
51. Saito, K., et al., *Detailed deposition density maps constructed by large-scale soil sampling for gamma-ray emitting radioactive nuclides from the Fukushima Dai-ichi Nuclear Power Plant accident.* Journal of environmental radioactivity, 2015. **139**: p. 308-319.

APPENDIX A – SIMULATION PARAMETERS

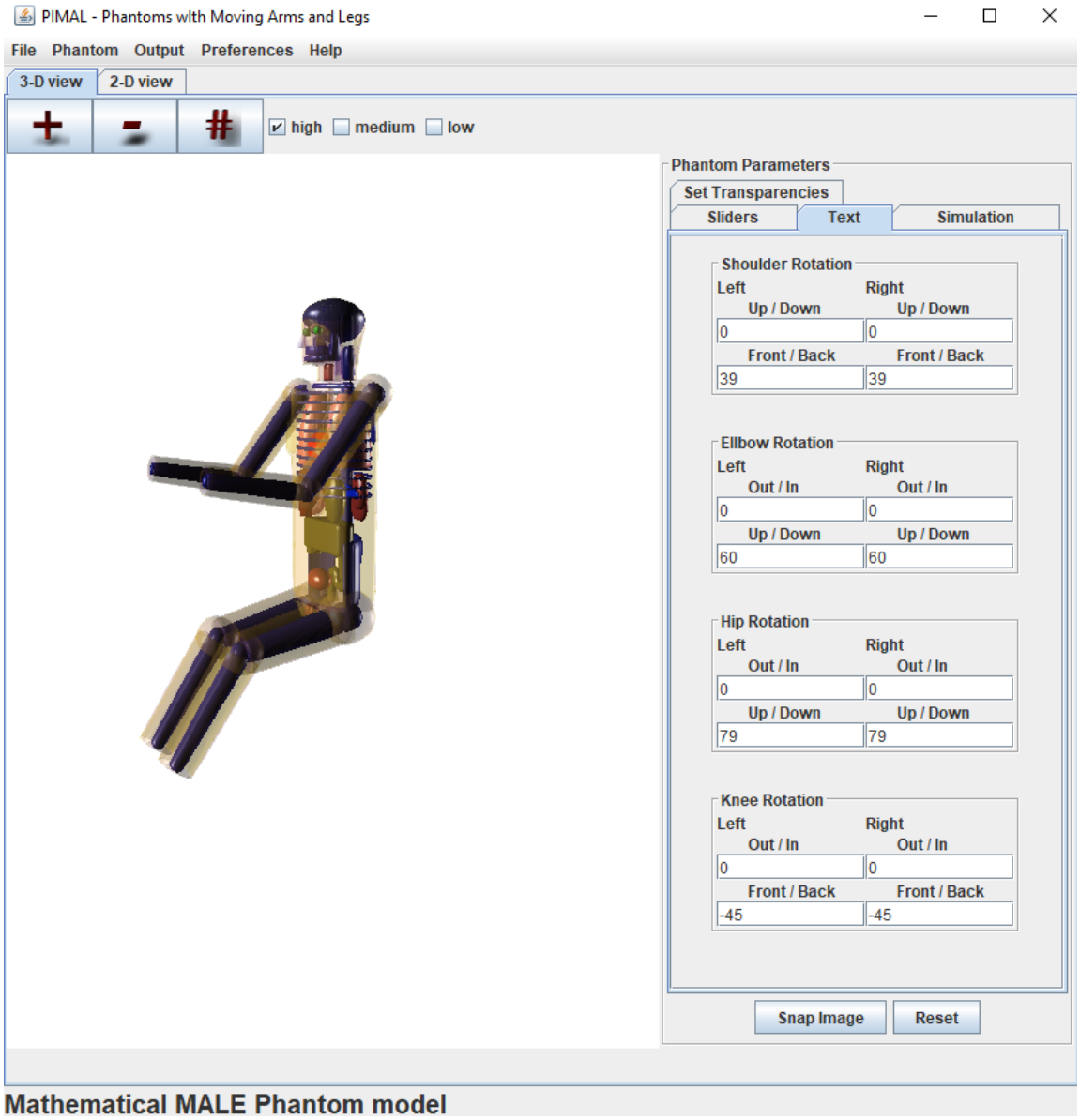

Figure A-1. PIMAL mathematical phantom model used as a representative driver.

Table A-1. Fiberglass composition used in vehicle window.

Element	Mass Fraction
B	0.018579
O	0.478631
Na	0.059171
Mg	0.018037
Al	0.021107
Si	0.302924
S	0.000399
Ca	0.099757
Fe	0.001395

Table A-2. Steel composition used for Type A package.

Element	Mass Fraction
Si	0.01000
Cr	0.19000
Mn	0.02000
Fe	0.68000
Ni	0.10000

Table A-3. Carbon Steel composition used for vehicles.

Element	Mass Fraction
Fe	0.99500
C	0.00500

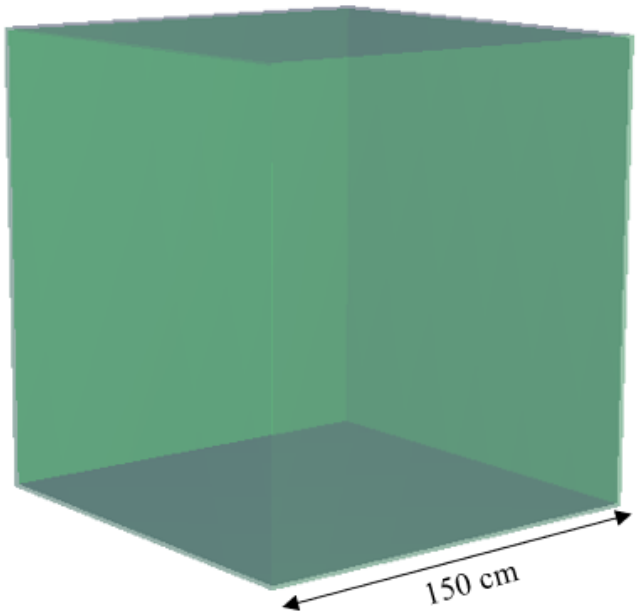

Figure A-2. 1-cm-thick and 1-in-thick box model.

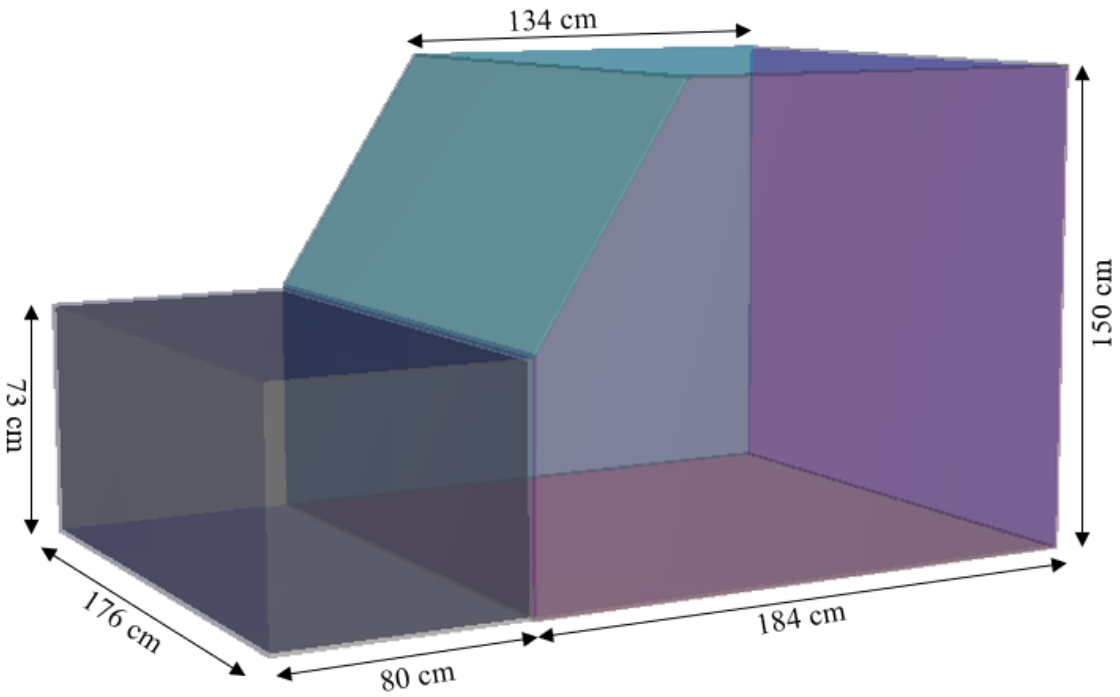

Figure A-3. More realistic vehicle model.

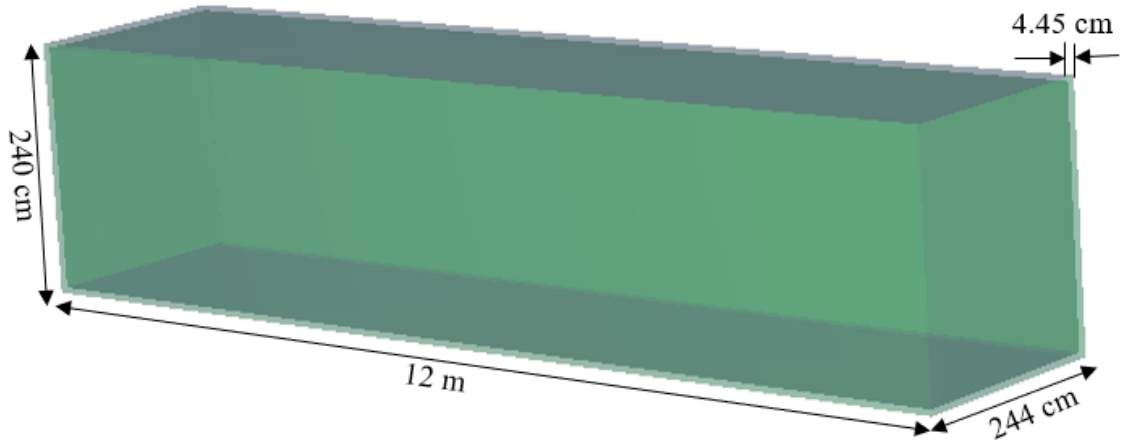

Figure A-4. Truck-trailer model.

Table A-4. Photon energy and intensity data for generated radionuclides.

Radionuclide	Photon Energy (MeV)	Intensity (%)
^{22}Na	1.27453	99.944
^{60}Co	1.17323	99.85
	1.33249	99.9826
^{85}Kr	0.513997	0.434
^{91}Sr:^{91m}Y	0.7498	23.6845
	1.0243	33.5
^{95}Nb	0.765803	99.808
^{95m}Nb	0.204116	2.296
	0.23569	24.366
^{95}Zr:^{95}Mo	0.724192	44.27
	0.756725	54.38
^{99m}Tc:^{99}Mo	0.140511	89.0567
^{97}Zr:^{97}Nb	0.74336	93.06
^{103}Ru	0.497084	91.00
^{106}Ru:^{106}Rh	0.511861	20.4
	0.62193	9.9348
^{125}Sb	0.427874	29.8
	0.600597	17.7668
^{127}Te	0.4179	0.99
^{129}Te	0.4596	7.7
^{129m}Te	0.69588	3.0712
^{131}I: ^{131m}Te	0.284305	6.1357
	0.364489	81.7
	0.636989	7.1733
^{132}I: ^{132}Te	0.667718	98.7
	0.7726	75.6042
^{134}Cs	0.604721	97.6197
	0.795864	85.5297
^{136}Cs	0.818514	99.704
	1.04807	79.7632
^{137}Cs:^{137m}Ba	0.661657	89.7393
^{140}Ba	0.029966	14.0974
	0.16266	6.2195
	0.537261	24.39
^{140}La	0.487021	45.5058
	1.59621	95.4
^{141}Ce	0.145443	48.29
^{144}Ce:^{144}Pr	0.133515	11.09

Table A-4. Photon energy and intensity data for generated radionuclides.(continued)

Radionuclide	Photon Energy (MeV)	Intensity (%)
^{147}Nd	0.091105	27.9
	0.319411	1.953
	0.531016	13.0851
^{148}Pm	0.55027	22.0002
	1.46512	22.2
^{148m}Pm	0.55027	94.8721
	0.62997	88.9982
	0.7257	32.8403
^{154}Eu	0.123071	40.5569
	1.27444	34.993
^{156}Eu	0.81177	9.7
	1.23071	7.9831
	2.2699	1.0311
^{192}Ir	0.316506	82.7105
	0.468069	47.8103
^{226}Ra	0.186211	3.59
^{235}U	0.14376	10.96
	0.185715	57.2
^{239}Pu	0.012975	0.0337
^{241}Am	0.059541	35.9
^{252}Cf	0.44	2.5333
	0.54	1.9667
	1.1	3.9333
	1.56	2.4
	2	1.26667
	2.4	1.02